THE UNIVERSITY OF MICHIGAN
INDUSTRY PROGRAM OF THE COLLEGE OF ENGINEERING

MEASUREMENT OF THE g-FACTOR ANOMALY OF FREE, HIGH ENERGY ELECTRONS

Arthur August Schupp, Jr.

A dissertation submitted in partial fulfillment
of the requirements for the degree of
Doctor of Philosophy in the
University of Michigan
1959

August, 1959

IP-377

Doctoral Committee:

Professor H. Richard Crane, Chairman
Professor Robert C. Bartels
Professor Kenneth M. Case
Assistant Professor Peter A. Franken
Professor Robert W. Pidd
Professor Marcellus L. Wiedenbeck

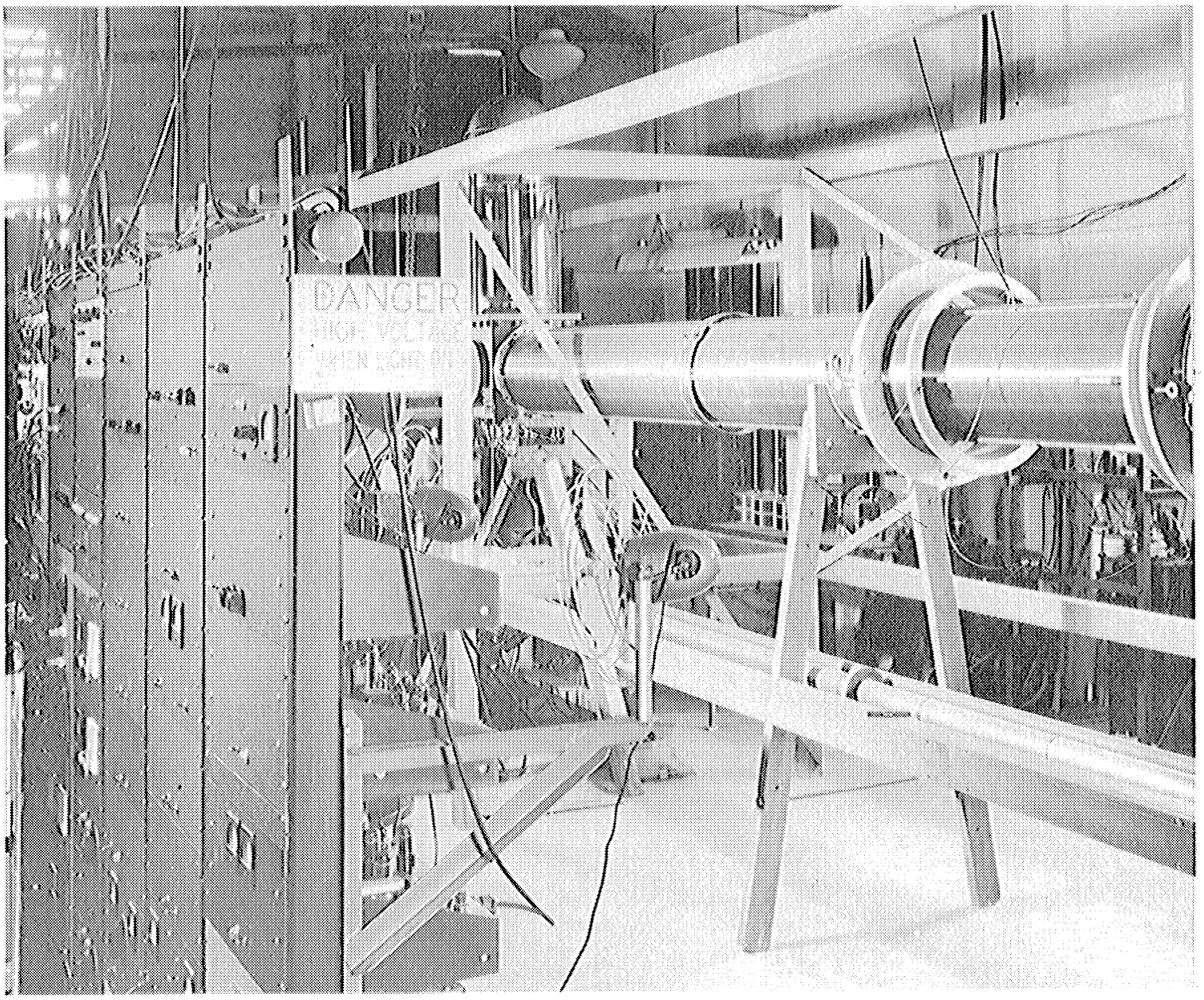

Overall View of Experimental Apparatus

ACKNOWLEDGEMENTS

The author wishes to express his appreciation to the chairman of his committee, Dr. H. R. Crane, and to Dr. R. W. Pidd, for their encouragement throughout this work as well as their many helpful ideas and suggestions about the experiment. The author also wishes to thank Mr. H. A. Westrick for his cooperation and skill in the design and construction of much of the apparatus, to the graduate students who also helped in the construction and assembly of the apparatus, to his wife for her cooperation and patience, and to his father for his encouragement throughout the course of this work.

The author wishes to express his appreciation to the United States Atomic Energy Commission for support of this work under Contract No. AT(11-1)-70, and to the Industry Program of the College of Engineering for the typing and printing of this thesis.

TABLE OF CONTENTS

TABLE OF CONTENTS (CONT'D)

LIST OF TABLES

LIST OF FIGURES

LIST OF FIGURES (CONT'D)

I. INTRODUCTION

Review of Electron g-Factor and Magnetic Moment Experiments

The gyromagnetic ratio is defined as the ratio of the magnetic moment of a body to its angular momentum. Classically, for all bodies with the same charge to mass ratio throughout, the gyromagnetic ratio is

$$G = e/2m$$

where e is the charge on the body and m is the mass of the body. For a quantum mechanical particle, in this case the electron, the gyromagnetic ratio has to be modified to account for relativistic and quantum electrodynamic effects and can be written

$$G_e = g_e e/2m = (1 + a) e/m$$

where g_e is a dimensionless quantity called the g-factor of the free electron and a is called the g-factor anomaly.

It is the purpose of this dissertation to report on a precision determination of the electronic g-factor anomaly by a measurement on high energy, unbound electrons. This quantity provides one of the few experimental checks on the present theory of quantum electrodynamics which predicts an infinite series of radiative correction terms to the Dirac value of 2 for the g-factor of the free electron. The difficulty in checking the results of this theory arises from the fact that the radiative corrections are small compared to the results of semiclassical theory and thus have been checked only by the Lamb shift and magnetic moment measurements on low energy, bound electrons.

In 1947, Lamb and Retherford[1] showed experimentally that the $2^2S_{1/2}$ state of atomic hydrogen did not coincide exactly with the $2^2P_{1/2}$

state as predicted by Dirac theory[2]. This was the first conclusive evidence of a difference between experiment and the existing theory and signaled the introduction of quantum electrodynamics to resolve the differences. About a month after this discovery Bethe[3] reinterpreted the existing quantum electrodynamic theory and was able to explain the Lamb shift. By subtraction techniques he removed the divergences of the theory and found that the $2^2S_{1/2}$ state of hydrogen should be 1040 megacycles above the value due to Dirac theory. This value is in good agreement with the experimental value of 1000 megacycles and demonstrated the applicability of quantum electrodynamics. At about the same time Breit[4] suggested that the deviations of the level splitting of the hyperfine structure of the ground state of hydrogen and deuterium for zero magnetic field[5,6] could be accounted for by postulating the existence of an anomalous magnetic moment for the electron. He found that the theoretical predictions would agree with experimental evidence if the magnetic moment of the electron was slightly larger than one Bohr magneton as predicted by Dirac theory.

In 1948, Schwinger[7,8] showed that the magnetic moment and g-factor of the free electron is modified by the quantization of the electromagnetic field. The g-factor is expressed as a series of radiative correction terms added to the Dirac value of 2. These terms are expressible in powers of the fine structure constant[9]

$$\alpha = e^2/\hbar c = 7.29719 \times 10^{-3}$$

The first of these terms, the first order in α, was calculated by Schwinger and he found that the g-factor for the free electron should be

$$g_e = 2(1+\alpha/2\pi) = 2(1.0011638)$$

The second order term in α, has been evaluated by Karplus and Kroll[10] and by Sommerfield[11]. The results are

$$g_e = 2(1+\alpha/2\pi - 2.973\alpha^2/\pi^2) = 2(1.0011454) \qquad \text{(Karplus - Kroll)}$$

$$g_e = 2(1+\alpha/2\pi - 0.328\alpha^2/\pi^2) = 2(1.0011596) \qquad \text{(Sommerfield)}$$

Recently this difference has been resolved and the accepted value is 2(1.0011596). It is also in agreement with the bounds calculated by Petermann.[12]

Since then a number of experiments have been completed that determine the magnetic moment and g-factor of an electron when bound in an atom. Kusch and Foley[13] have shown that $g_e = 2(1.00119 \pm 0.00005)$ by atomic beam measurements of the Zeeman effect in the ground state of Ga, In, and Na. A more precise determination of the g-factor can be achieved by performing two separate experiments. One experiment determines the magnetic moment of the proton in units of the Bohr magneton (μ_p/μ_o), and the other experiment determines the ratio of the magnetic moment of the electron to the magnetic moment of the proton (μ_e/μ_p). The product of these two results gives the magnetic moment in units of Bohr magnetons or one-half the g-factor for the bound electron. By applying suitable relativistic corrections the magnetic moment of the free electron can be obtained.

In 1949, Taub and Kusch[14] made the first determination of (μ_e/μ_p) by a molecular beam magnetic resonance method. They measured the frequency corresponding to a reorientation of the proton in the molecule NaOH and the frequency corresponding to a transition between

certain of the hyperfine structure levels of the ground state of both Cs^{133} and In^{115}. By combining this result with measurements obtained in related experiments[13,15] they found that

$$\mu_e/\mu_p(NaOH) = 658.21 \pm 0.03$$

By observing the ratio of the electronic-spin g-value of atomic hydrogen in the $^2S_{1/2}$ state to the proton g-value in a sample of mineral oil or water the most precise values of (μ_e/μ_p) for a bound state are obtained. A relativistic correction is applied to account for the binding energy of the electron in the hydrogen atom and then (μ_e/μ_p) for the free electron is obtained. Three results have been published by different groups[16-18] using the above methods and the results are all in agreement to within two parts per million. The average of their results yield

$$\mu_e/\mu_p(Oil) = 658.2292 \pm 0.0012$$

A determination of $\mu_p(Oil)/\mu_o$ has been completed by Gardner and Purcell[19] and independently by Franken and Liebes[20]. In these experiments, the ratio of the nuclear magnetic resonance frequency of protons to the cyclotron frequency of free low energy electrons was determined. Both frequency determinations were performed, as nearly as possible, in the same location in the magnetic field so that a measurement of the magnetic field was not necessary. The results of these experiments were

$$\mu_o/\mu_p(Oil) = 657.475 \pm 0.008 \qquad \text{(Gardner - Purcell)}$$

$$\mu_o/\mu_p(Oil) = 657.462 \pm 0.003 \qquad \text{(Franken - Liebes)}$$

When these results are combined with the value for μ_e/μ_p(Oil) the following values for the g-factor are obtained

$$g_e = 2(1.001146 \pm 0.000012) \qquad \text{(Gardner - Purcell)}$$

$$g_e = 2(1.001168 \pm 0.000005) \qquad \text{(Franken - Liebes)}$$

The Gardner and Purcell measurement is considerably below the present theoretical value of 2(1.0011596) and has been recently remeasured by Hardy and Purcell[21] with the result that

$$g_e = 2(1.0011561 \pm 0.0000015) \qquad \text{(Hardy - Purcell)}$$

In all of the above experiments the g-factor of the free electron was obtained by a combination of two different experiments. This was necessary to eliminate a common factor, the magnetic moment of the proton in mineral oil, so that the magnetic moment of the electron in units of Bohr magnetons could be obtained. To find the g-factor for free electrons a correction term had to be considered that would account for the electron binding energy. For these reasons and others, some systematic differences between results on bound and on free electrons may be present, thus making a measurement of the g-factor directly on free electrons highly desirable. A measurement at high energies would also be desirable to further check the relativistic effects and the applicability of quantum electrodynamics.

A number of proposals have been advanced for experimentally measuring the g-factor of free electrons. One such experiment, as proposed by Bloch[22], is based on magnetic resonance techniques on slow electrons in a magnetic field. Here electrons are sorted and trapped

by electric and magnetic fields such that only electrons in the lowest magnetic state are trapped. A weak oscillating electric and magnetic field is then applied to induce transitions to higher states and cause the electrons to leave the trap and be detected. Two resonant frequencies should be found, one corresponding to a spin transition and the other corresponding to an orbital transition. The g-factor of the free electron is equal to twice the ratio of these frequencies. Another group of experiments uses the double scattering process with a magnetic field between the first and second scatterer. The theory of the double scattering process has been worked out in detail by Mott[23] and shows that a beam of electrons is partially polarized, a partial alignment of the spins or magnetic moments, in a direction perpendicular to a plane formed by the incident beam and the beam after single nuclear scattering. If this beam is scattered again, the theory shows that there will be an azimuthal asymmetry in scattering due to the polarization of the beam. Many attempts have been made to observe this asymmetry and the most recent of these, by Nelson[24], gives excellent agreement with theory. Tolhoek and DeGroot[25] proposed an experiment using the double scattering process with a radio frequency field between the first and second scatterers. This field could be adjusted in frequency until the asymmetry after second scattering vanished indicating that the spin resonant frequency had been reached and the beam depolarized. This frequency and the magnetic field in which the beam was depolarized would then give the g-factor for the free electron. Another experiment using the double scattering process, proposed by Crane, Pidd and Louisell[26], has been completed as a thesis by Louisell[27]. In this experiment a magnetic

field is inserted between the first and second scatterers parallel to the electron's velocity. This field causes the polarization vector of the beam to precess and since the plane of maximum asymmetry depends on the polarization direction, this also precesses. Louisell showed that the g-factor can be obtained by a measurement of the magnetic field, electron energy, distance between the first and second targets, and the angle of rotation of the asymmetry. If the experimental conditions are such that there are many rotations of the asymmetry then the measurement of the angle of rotation can be very precise. Since only five revolutions of the beam were used in this experiment, the precision was limited to $\pm$ 1/2 percent and yielded

$$g_e = 2.00 \pm 0.01$$

This experiment was not accurate enough to show the radiative corrections but did prove the feasibility of making a direct measurement on free electrons.

Present Experimental Proposal

As seen from the previous discussion, a precision measurement of the g-factor of high energy, free electrons is highly desirable. The present experiment was, therefore, undertaken with a precision of a few parts per million in mind. The double scattering process is used with a beam energy of 100 kilovolts since the Mott asymmetry is near its maximum there. A magnetic field, produced by a solenoid, is interposed between the polarizer (first) and the analyzer (second) targets. This field is oriented in such a way that the electrons, before scattering, travel along a field line and scatter off the polarizer target so that the scattered beam is traveling at approximately ninety degrees to the

magnetic field. The polarization vector is initially normal to the plane through the incident and first scattered beam and, thus, pointing in the radial direction. Between the targets the beam will travel in a helical path and rotate at the cyclotron frequency while the polarization vector will precess slightly faster due to the anomalous magnetic moment of the electron.

The difference frequency, the precession frequency minus the cyclotron frequency, is the quantity that is measured directly by studying the intensity asymmetry after second scattering as a function of the time spent between scatterers. A schematic diagram of this experiment is shown in Figure 1. Since the precession frequency is slightly greater than the orbital frequency of the electron, the polarization vector will precess about the magnetic field and eventually become parallel to the direction of motion of the electrons. In this state, the asymmetry after second scattering will vanish. At a later time, the polarization vector will be opposite to the initial direction and the asymmetry will reverse. In this manner, a cosine curve can be traced whose frequency is the difference frequency. Mendlowitz and Case[28] have theoretically investigated the motion of an electron in a homogeneous magnetic field using the Dirac equation with the addition of a Pauli type term to account for the anomalous magnetic moment. These calculations show that

$$\omega_s = \omega_c \left(1 + a\sqrt{(1-\beta^2)^{-1}}\right)$$

when the electron velocity is perpendicular to the magnetic field. Rearranging this equation to give the g-factor anomaly a, we find

$$a = (\omega_s - \omega_c)(1-\beta^2)^{1/2}(\omega_c)^{-1} = \omega_D/\omega_0$$

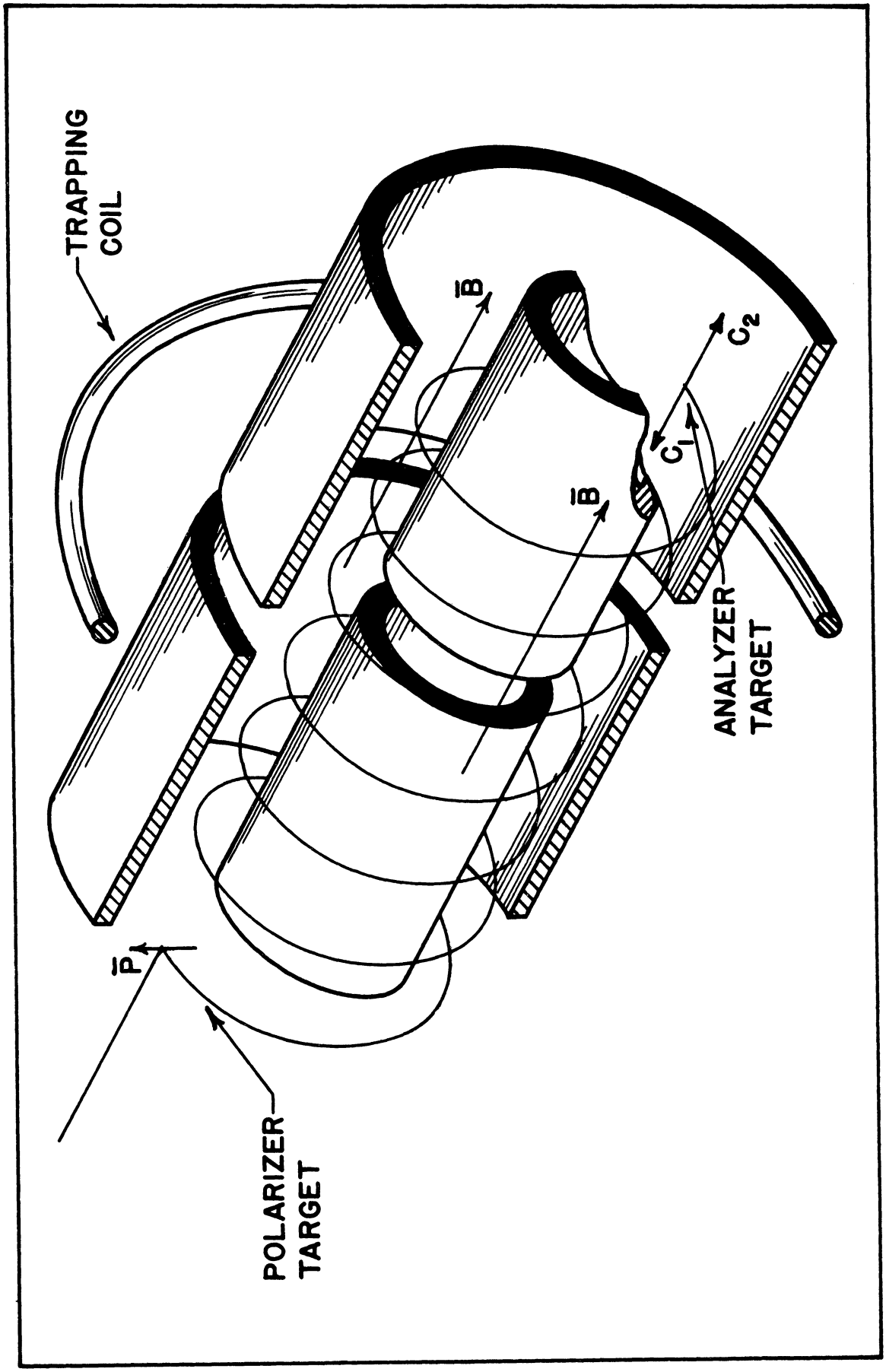

Figure 1. Schematic Diagram of the Experiment

where ω_D is the difference frequency $(\omega_s - \omega_c)$, ω_o is the zero energy cyclotron frequency (eB/m_o), e is the electron charge, B is the magnetic field, and m_o is the rest mass of the electron.

Since the g-factor anomaly is approximately one-thousandth of the g-factor, a determination of the difference frequency and the magnetic field to one part in a thousand will give the g-factor to about one part in a million. In order to determine the difference frequency accurately, a large number of revolutions are required which necessitates keeping the electrons in the magnetic field for a long period of time. This is accomplished by giving the magnetic field a slight betatron shape by the addition of the external trapping coil shown in Figure 1. Before the electron pulse enters the system, the second set of concentric cylinders (those nearest the analyzer target) are pulsed 100 volts negative. As the electron pulse crosses the gap between the two sets of cylinders, the momentum is reduced and some of the electrons will be reflected back towards the first target by the shaped magnetic field. Before these reflected electrons return to the gap, the voltage is removed and these electrons are then permanently trapped in the betatron field. At some later time the first set of concentric cylinders are pulsed negative giving those electrons on the polarizer side of the gap an additional 100 volts of energy as they cross the gap. These electrons will then leave the shaped field region and encounter the second target. In this way many cycles of the difference frequency can be observed and the period can be determined very accurately. The magnetic field must also be measured to a part in a thousand and this is accomplished by making the inhomogeneities small and measuring the field with a proton resonance device.

Results and Conclusions

The procedure just described has been successful in trapping electrons for more than 300 microseconds which corresponds to approximately 100 cycles of the difference frequency. The difference frequency has been determined to about 0.1 percent for electron energies between 50 and 100 kilovolts. Combining these results with the corresponding magnetic fields yields the following value for the g-factor anomaly

$$a = 0.0011609 \pm 0.0000021 = \alpha/2\pi - (0.1 \pm 0.4)\alpha^2/\pi^2$$

where the error represents the standard deviation in the measurement. This value is in excellent agreement with the current theoretical value of

$$a = \alpha/2\pi - 0.328\alpha^2/\pi^2 = 0.0011596$$

The data have also been evaluated, by assuming the theoretical value for the g-factor anomaly, to give an upper limit on the electric dipole moment of the electron of

$$3 \times 10^{-15} \text{ cm}$$ (times the electronic charge)

The principal sources of error are the determination of the effective magnetic field in the trapping region, the determination of the difference frequency, and the evaluation of the stray electric fields due to charging of the concentric cylinders in the trapping region.

II. APPARATUS

General Physical Layout

The apparatus necessary for the measurement of the g-factor anomaly consists of the following elements: 1) a source of electrons, including a high voltage supply and an electron gun; 2) a polarizer target; 3) a magnetic field; 4) field trimming coils; 5) trapping apparatus; and 6) analyzing and detecting equipment. The construction of each of these elements along with the relevant circuitry will be described in this chapter. The solenoid, field shaping coil, gun, and earth correction coils can be seen in the Frontispiece.

High Voltage Supply

The high voltage supply consists of a voltage doubling circuit capable of giving D.C. voltages to 120 kilovolts. Regulation of the high voltage is desirable, since the orbits depend on the beam energy, and is achieved by taking a signal from the precision resistor used for the high voltage meter, converting this signal to an A.C. signal by an electronic chopper, amplifying this signal by a high gain A.C. amplifier, and reconverting back to a D.C. signal. This signal is then used to control the primary voltage of the high voltage transformer. This circuit is capable of regulating the high voltage to $\pm$ 1 percent after allowing a suitable warm-up period. Since the regulating circuit is essentially a D.C. regulator, line voltage ripple and spikes in the high voltage due to corona discharges are not eliminated. These variations have been observed by placing an oscilloscope across the amplifier input and found to be $\pm$ 2 percent.

Electron Gun

The electron gun is designed to produce a pulsed beam of high peak current (approximately 100 milliamperes). It consists of a water-cooled, copper, cup-shaped cathode, 1 inch in diameter and 1-1/4 inches deep. The filament, placed 1/2 inch behind the rim of the cathode cup, is a flat spiral of four turns of 0.02-inch tungsten wire. This assembly is placed inside and insulated from the case of the gun which is machined from a section of 2-inch diameter aluminum pipe. The gun case is supported on glass insulators at one end, and from the top of a 16-inch diameter glass cylinder at the other end. The top of the glass cylinder and the gun are connected to the high voltage supply so that the complete assembly is at -100 kilovolts. This assembly is shown in Figure 2.

The cathode assembly is insulated from the gun case so that it can be biased 500 volts positive with respect to the case structure (acting like a grid) and, thus, keep the gun cut off. A negative 4000 volt pulse, 0.13 microseconds wide is generated by a thyratron pulser and applied to the cathode assembly. This causes a pulse of electrons to be accelerated through the grid structure into the 100 kilovolt field between the gun structure and ground. The beam current is measured by placing a collector cup in the beam path and calculating the peak current from the average value obtained.

Beam Deflecting and Focusing Coils

The electron beam diverges as it passes through the accelerating gap and must be focused on the polarizer target about 50 inches in front of the gun. Partial focusing is provided by the main solenoid field, but an additional focusing field is needed since the main solenoid

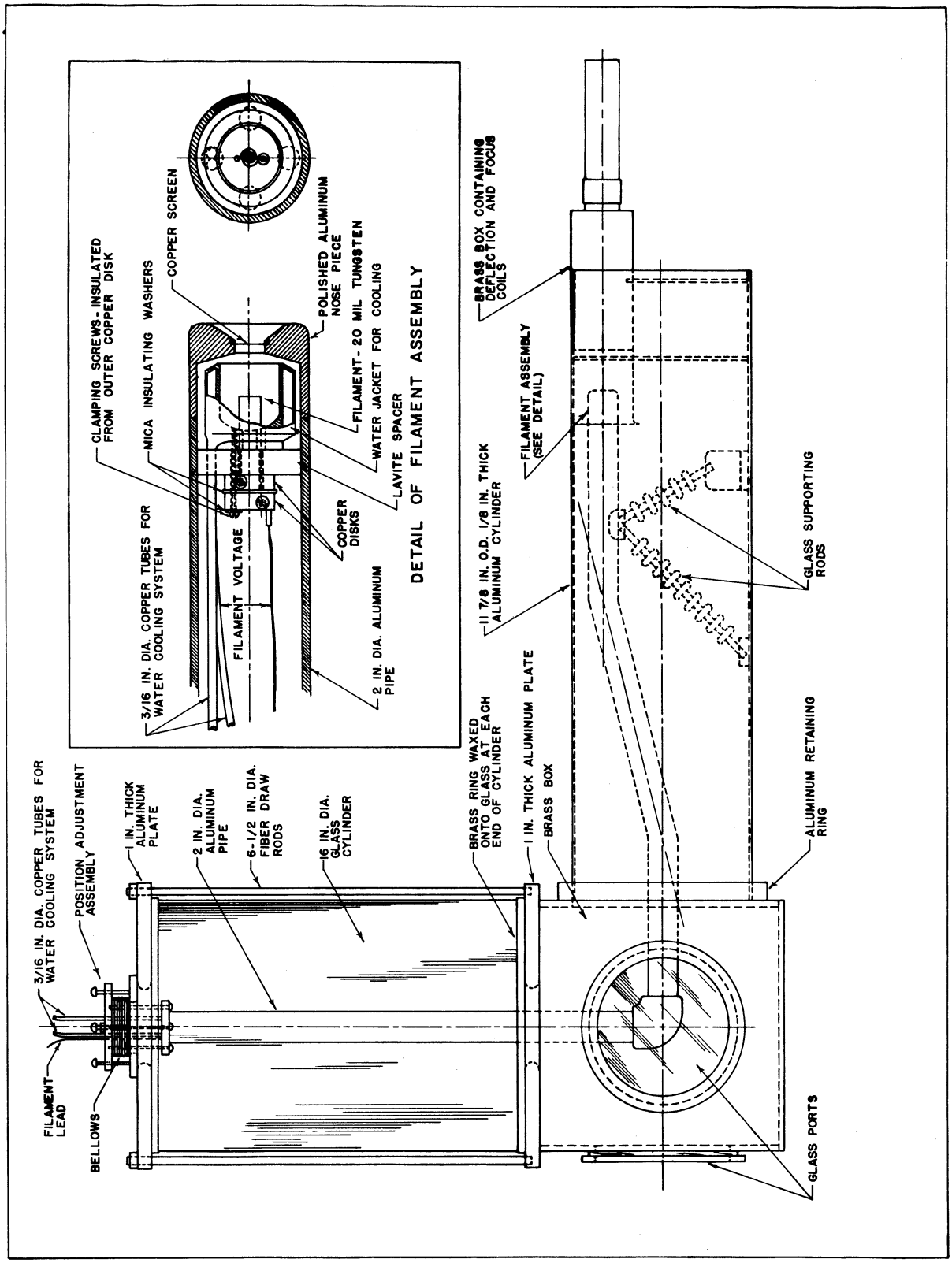

Figure 2. Drawing of the Gun Assembly

is varied during the course of the g-factor anomaly measurement. This additional field is provided by a small solenoid 10 inches long and 2 inches in diameter, wound with 4000 turns of #28 magnet wire. In order to correct for any misalignment of the gun with respect to the polarizer target, horizontal and vertical deflection coils are also necessary. These coils consist of two sets of two coils 3-1/2 inches wide and 8 inches long, wound with 500 turns each of #26 wire. These three sets of coils are located in a vacuum-tight box just in front of the gun as shown in Figure 2, and are supplied by regulated current supplies.

Polarizer Assembly

The polarizer assembly consists of a slit to restrict the incident beam, a target wheel, and a second slit to restrict the scattered beam. The target wheel is movable from outside the vacuum system and has four positions. These four positions contain a gold polarizer target which produces the polarized beam, an aluminum target which produces an unpolarized beam necessary for studying possible spurious instrumental asymmetries, a blank target holder used to study background counting rates, and a collector cup used to monitor the beam intensity. The polarizer assembly can be seen in the photograph of the complete assembly shown in Figure 4.

Solenoid

The solenoid is wound on an aluminum form made from two 10-foot sections of 12-inch inside diameter pipe, which also serves as the vacuum chamber. The winding consists of four layers of #10 heavy Formvar magnet wire, close-wound with 2160 turns per layer. For this

experiment, the four layers are connected in series and produce a field of approximately 107 gauss at the center with a current of 6 amperes. Regulation of the magnetic field is necessary since the anomalous g-factor is inversely proportional to the field and is accomplished by passing the solenoid current through a bank of 48 power triodes (6AS7's) connected in parallel. The triodes are controlled by the output of a high gain D.C. difference amplifier whose input voltages are a reference voltage and a voltage proportional to the solenoid current. The solenoid current is monitored by a diode that is sensitive to magnetic fields (G. E. 2B23) placed in an auxiliary coil in series with the solenoid. The plate (current) voltage of this diode is proportional to the solenoid current and is used as the input signal for the difference amplifier. The regulator is capable of eliminating ripple to better than 0.1 percent and has a drift rate of less than 0.05 percent per hour.

The current in the solenoid was set by monitoring the voltage across a standard shunt with a precision potentiometer. In this manner the current could be set to about 0.1 percent. The potentiometer was calibrated by measuring the magnetic field with a proton resonance device. Corrections were applied to account for the component of the earth's magnetic field along the solenoid axis.

Earth Correction Coils

The horizontal and vertical components of the earth's magnetic field within the trapping region are cancelled by two sets of correction coils. These coils are wound with 30 turns each of #14 heavy Formvar magnet wire in wooden forms 28.25 feet long and 5 feet wide. They produce a uniform field of 0.16 gauss per ampere, and are supplied by a

regulated current. The current is regulated by circuits identical to the solenoid regulator and have an error of ± 0.1 percent.

Field Shaping Coil

The uniform field of the solenoid must be shaped to produce a trapping field (betatron field) for the electrons. This is accomplished by the addition of an external coil 18 inches in diameter, 6 inches wide, with 593 turns of #30 magnet wire, wound in a single layer. The current in this coil is regulated by a chopper stabilized D.C. amplifier circuit, and holds the field to ± 0.001 gauss at the center of the coil. The radial and axial components of the field were calculated by graphical integration of the field components due to a single loop. The calculated values are shown in Appendix II, Part A. These components were added to the calculated components of the solenoid field, and are shown in Figure 7.

Trapping Assembly

The magnetic field shown in Figure 7 is designed to trap any electrons that are reflected by the betatron-shaped field. Actually, all electrons entering the shaped field will gain enough energy as they approach the center of the betatron field so that none will be trapped unless they lose some axial momentum while in this region. The momentum of the electrons is decreased by applying an injection (decelerating) voltage pulse across a 1/4-inch gap at the center of the trapping region. Some of the electrons will now be reflected back towards the polarizer target. The injection pulse is removed before the electrons get back to the gap so that the loss of energy is permanent and the electrons are

trapped. After a predetermined time (trapping time), an ejection (accelerating) voltage pulse is applied across the gap and the energy of the electrons is restored. The electrons then leave the trap and strike the analyzer target.

The mechanical construction of the entire trapping apparatus including targets and counters, is shown in the drawing in Figure 3 and in the photograph in Figure 4. This apparatus consists of three sets of two concentric cylinders of 9-1/4 inches in diameter, and 5-3/4 inches in diameter. The first two sets (the set nearest the polarizer target and the center set) are insulated from ground, and the third set is grounded. The second set is pulsed negative to decelerate the electrons and the first set is pulsed negative to accelerate and eject the electrons. The timing and control of these pulses will be described in a following section.

Analyzer Assembly

The analyzer assembly consists of a target holder and three geiger counters. The target holder contains two targets, a gold and an aluminum foil, that can be lowered into the path of the circulating beam from outside the vacuum. Slits before the target restrict the beam to a radial spread of 1/4 inch. The targets are supported at one point only from outside the beam radius so that there is no scattering off the target holder. Three geiger counters are used to detect the scattered beam, two at an 80° scattering angle for measurement of the asymmetry, and one at 15° as a monitor of the beam intensity. These counters are standard end window geiger counters, 2-1/2 inches long with an inside diameter of 1/2 inch. The central wire, a piece of 0.005-inch diameter

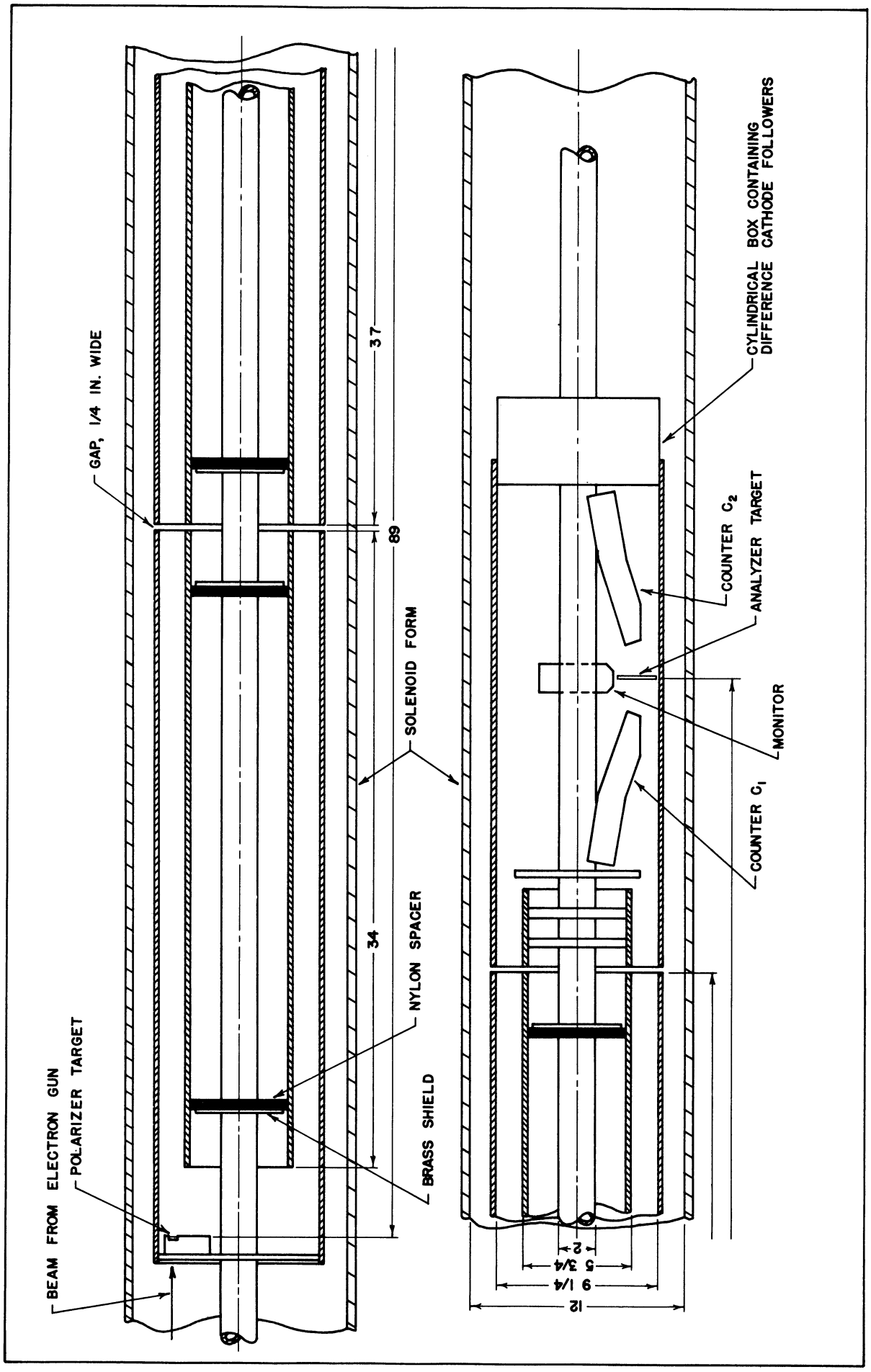

Figure 3. Drawing of the Trapping Assembly

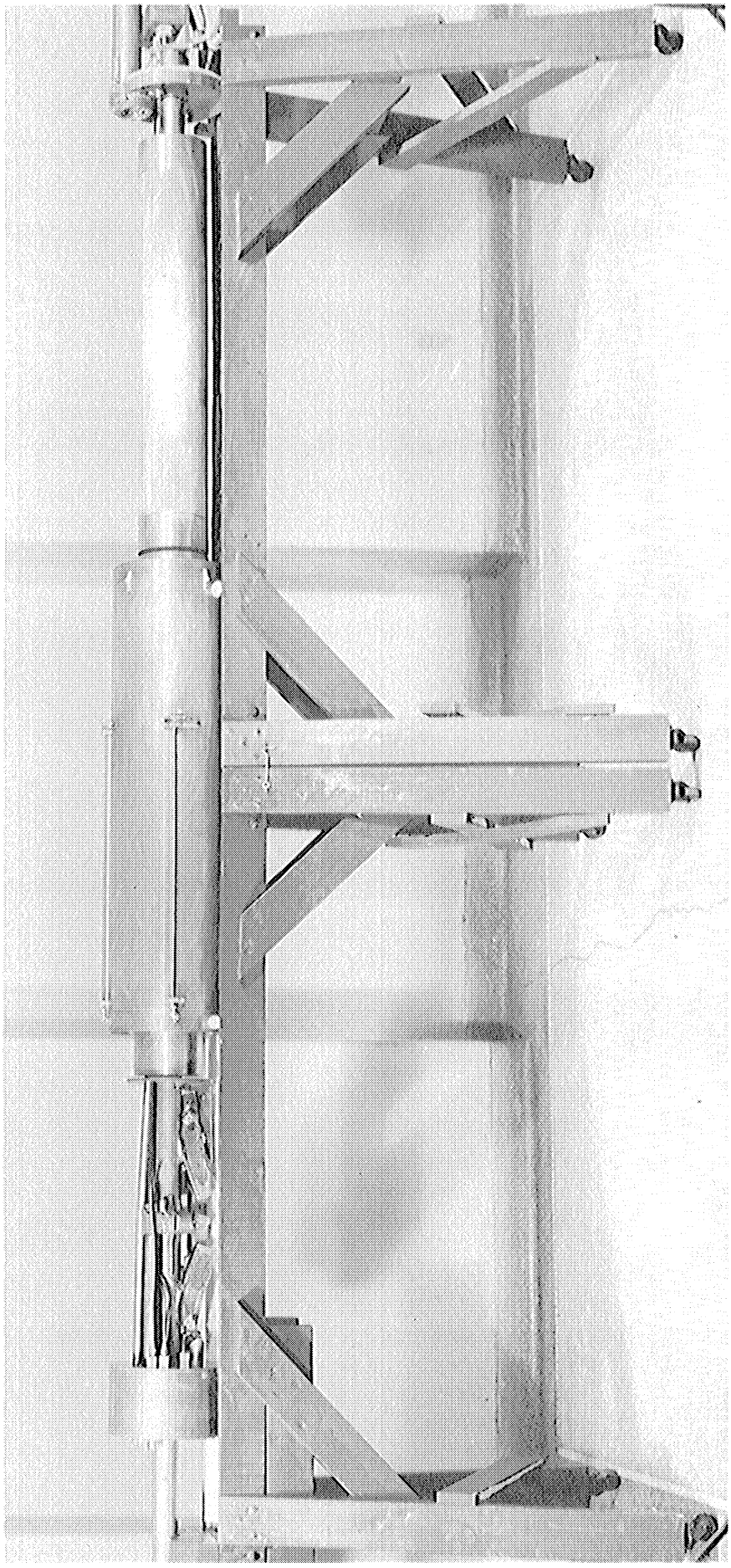

Figure 4. Photograph of the Trapping Assembly

tungsten wire, is supported at one end by a glass insulator and is beaded at the other. The window is made from a piece of aluminized milar film 0.00025 inches thick.

Control Circuitry

The sequence of events is: 1) the injection pulse is applied to the second set of cylinders, 2) the gun emits a pulse of electrons, 3) the injection pulse is removed, 4) the geiger counters are pulsed into the operating region, 5) the ejection pulse is applied to the first set of cylinders, 6) the counting circuit gates are opened, and 7) the ejection pulse is removed. This cycle is repeated a thousand times each second. A block diagram of the system is shown in Figure 5. The timing circuit is a crystal-controlled circuit that generates two main pulses separated by an adjustable number of 1/2 microsecond steps. This circuit will be described in detail in the next section of this chapter. The first of these pulses (1) drives a thyratron pulser that transmits a signal up to circuits riding at -100 kilovolts. Here the pulse is reshaped and used to drive another thyratron pulser that generates a 0.13 microsecond, 4000 volt high pulse for the gun. This pulse is delayed and clipped to 3000 volts before reaching the cathode of the gun. The time relationship between the gun pulse and the injection pulse is very critical, and jitter is greatly reduced by triggering the injection pulse circuits directly from the gun pulse, thus, eliminating any jitter due to the transmission of the timing pulse and thyratron pulser. This is accomplished by returning the gun pulse, before the delay line, to ground potential through a 150 kilovolt condenser and using this pulse to trigger the injection pulse circuits. A 0-1 microsecond variable delay line

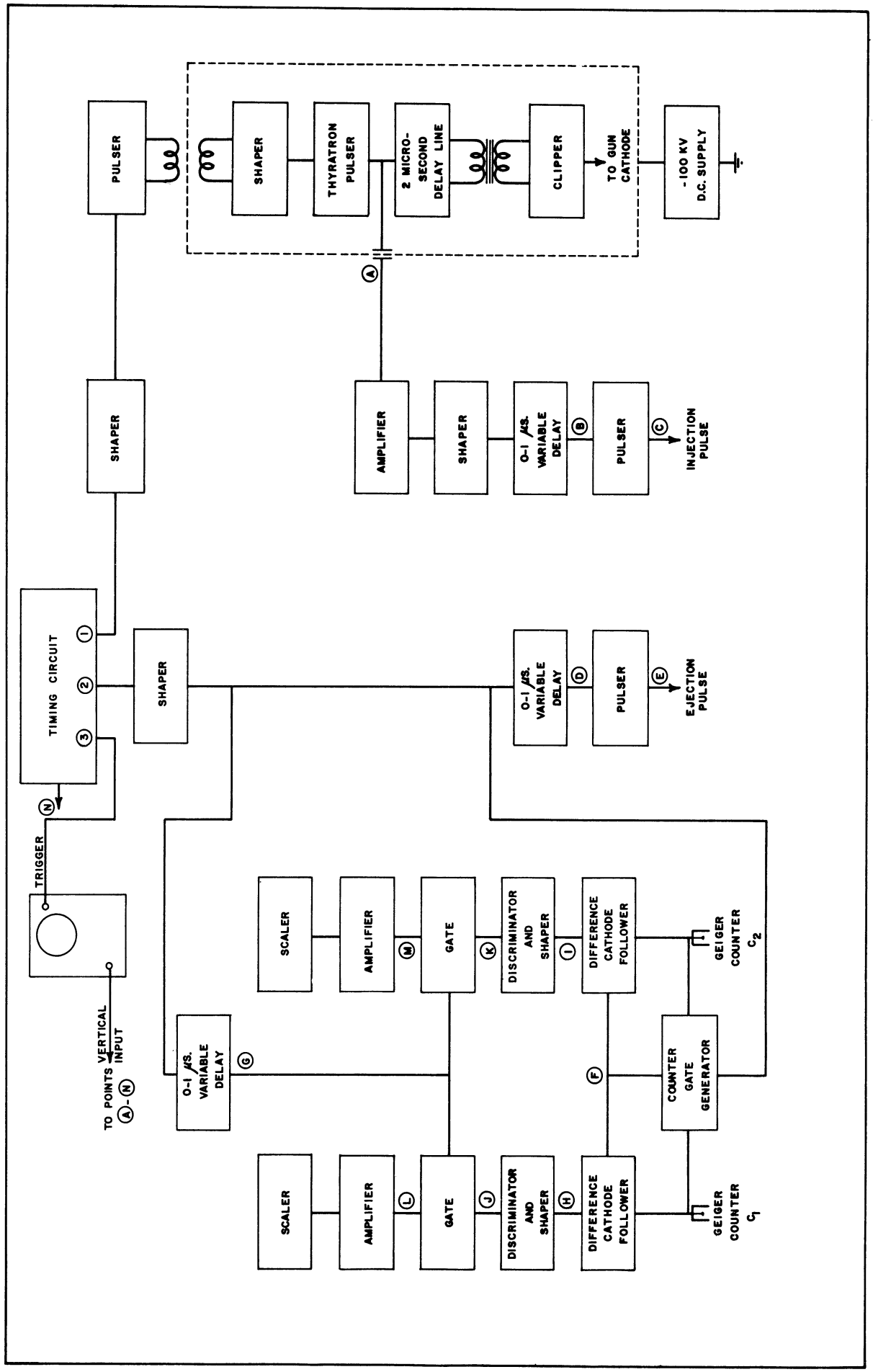

Figure 5. Block Diagram of Control Circuitry

is used to accurately adjust the time of the injection pulse with respect to the gun pulse. The injection pulse is a pulse 0.5 microseconds wide and 100 volts high with a rise time of 0.03 microseconds, generated by a delay line pulser. The second pulse from the timing circuit (2) can be adjusted in time with respect to the first from 0 to 999.5 microseconds, and controls the length of the trapping duration. This pulse turns on the counting circuits to be described later and also turns on the ejection pulser which is identical to the injection pulser. A variable delay line is inserted just before the pulser so that the timing of the counting circuits can be varied with respect to the ejection time of the electrons.

Timing Circuit

The timing circuit block diagram is shown in Figure 6. This circuit is a very accurate delay pulse generator controlled by a one-megacycle crystal oscillator with an accuracy of 0.01 percent. The oscillator is followed by a shaper that generates both a positive and a negative pulse 0.06 microseconds wide and 40 volts high. This pulse drives the first of three scales of ten circuits, using Burroughs Magnetic Beam Switching tubes (6700). This tube has ten outputs that can be selected by a switch so that a pulse is obtained when the beam is formed on the selected anode. The output from the tenth (zero) anode is fed into a coincident circuit along with the pulses from the master oscillator so that the output is a pulse in phase with the master oscillator, but delayed by ten microseconds. This pulse drives another scale of ten, identical with the first, which gives an output pulse in phase with the master oscillator but separated by 100 microseconds. A third

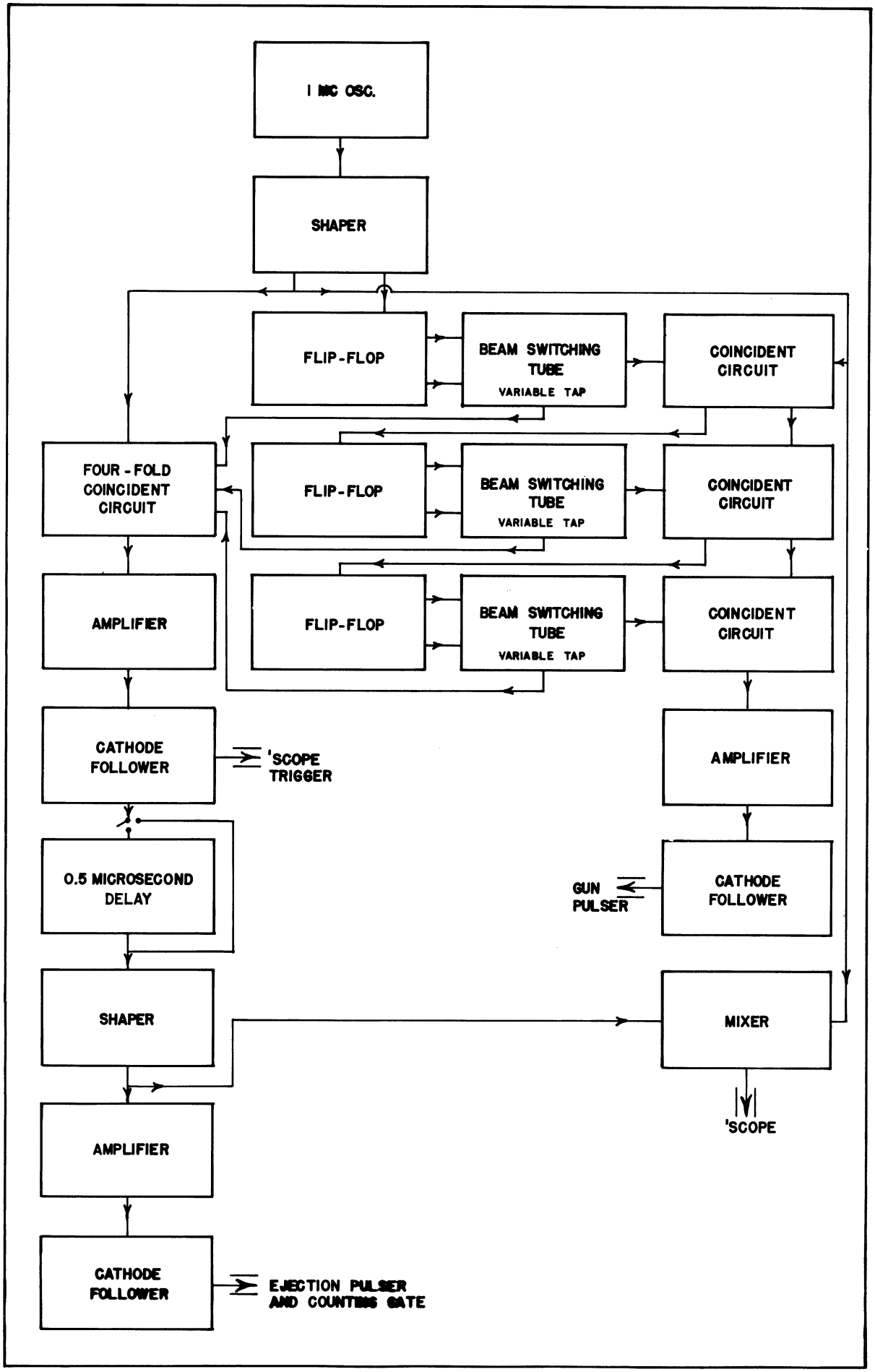

Figure 6. Block Diagram of Timing Circuit

circuit, identical to the first two, gives a total scale of 1000. The coincident circuits are necessary to eliminate any delay time due to the circuits. The adjustable output from each scale of ten is fed into a four-fold coincident circuit with the master oscillator pulses, and when there is a coincidence between all four pulses an output pulse is obtained. In this manner, any pulse from 0 to 999 microseconds delay with respect to the pulse from the tenth anode of the last scale of ten circuit is obtained. The half microsecond steps are obtained by switching in or out a fixed 1/2 microsecond delay line before the pulse is shaped. This delayed pulse controls the counter gate circuits and the ejection pulse applied to the first set of cylinders. A mixer circuit mixes the pulses from the master oscillator with the zero time pulse and the delayed pulse for monitoring with an oscilloscope.

Counting Circuits

The counting circuit block diagram is shown in Figure 5. The geiger counters are pulsed into the operating region about 0.2 microseconds before the beam is ejected. This time is controlled by the variable delay line just before the ejection pulser. Pulsing of the geiger counters is necessary because a large number of electrons enter the counter from the part of the injection beam that is not trapped. These electrons render the geiger counters inoperative during their dead time of about 100 microseconds, and would make it impossible to take data for trapping times less than the dead time. This trouble is eliminated by keeping the geiger counters just below their threshold voltage so that entering electrons do not cause a geiger discharge. The pulses from the geiger counters contain both the wanted geiger pulse plus the applied

pulse necessary to turn the counters on. This pulse is fed into a difference cathode follower along with the applied pulse and the difference, just the geiger pulse, is obtained between cathodes at a low output impedance. These circuits are situated as close as possible to the geiger counters so that any capacity to ground will be minimized. The outputs are fed into a discriminator circuit through a shielded balanced line and then shaped. Another gate circuit is added to insure counting only pulses that occur during a short period of time after the ejection pulse is applied. The output from the gate is amplified and then fed into the scalars.

III. APPARATUS STUDIES

Trapping Procedure

Trapping the electron beam was accomplished in two main steps. First, the trapping duration was set for approximately 5 microseconds since trapping durations of this length are insensitive to small changes in the solenoid current, field shaping coil current, and injection pulse voltage. This allowed adjustment of the beam on the polarizer target by changing currents in the deflecting and focusing coils until the counting rate was maximized. Rough adjustment of the solenoid current, shaping coil current, trapping voltage, and turn off time of the injection pulse with respect to the gun pulse could also be made at the same time. The second step was to slowly increase the trapping duration and make slight adjustments in the above parameters to maximize the counting rates. The main adjustments necessary were the field shaping coil current, the timing of the injection pulse, and placement of small shim magnets.

Two small permanent magnets were used to shim the solenoid field and were placed before the trapping region near the polarizer target. The field of these magnets is essentially a dipole field, and was less than 10^{-5} webers per square meter in the beam path as determined by the proton resonant device. Since the electrons only passed the region of the magnets once as they were entering the trapping region, it is believed that the magnets perturbed the initial beam direction in such a way that successful trapping was possible. In the trapping region the field of these magnets has fallen off to approximately 10^{-8} webers per square meter, and is completely negligible compared to the solenoid field of about 10^{-2} webers per square meter.

By careful adjustment of all the parameters, a good beam can be trapped for periods of 600 microseconds. After obtaining a trapped beam, the field shaping coil current is slowly reduced, while adjustments are made on the other parameters until the minimum possible current is reached consistent with good trapping. This procedure reduces the field inhomogeneities to a minimum and, thus, simplifies the procedure for calculating the average magnetic field in the trap.

Magnetic Field

An accurate determination of the magnetic field within the trapping region is necessary since the g-factor anomaly is inversely proportional to the average magnetic field encountered by the beam as it passes between the two targets. The field of the solenoid was calculated by expanding the field on the axis in a power series of the radius. The axial and radial components are given by

$$B_z(\rho,z) = \sum_{n=0}^{\infty} \frac{(-1)^n}{(n!)^2} B_z^{(2n)}(0,z) \left(\frac{\rho}{2}\right)^{2n} \tag{3.1}$$

$$B_\rho(\rho,z) = \sum_{n=0}^{\infty} \frac{(-1)^{n+1}}{(n!)^2(n+1)} B_z^{(2n+1)}(0,z) \left(\frac{\rho}{2}\right)^{2n+1} \tag{3.2}$$

where $B_z^{(n)}(0z)$ is the n^{th} derivative of the field on the axis of the solenoid

$$B_z(0,z) = \frac{\mu_0 NI}{2} \left[\frac{z+L}{\sqrt{(z+L)^2+R^2}} - \frac{z-L}{\sqrt{(z-L)^2+R^2}} \right] \tag{3.3}$$

where L = 2.896 meters is the half length, R is the winding radius, $\mu_o = 4\pi \times 10^{-7}$, N = 1492 is the number of turns per meter, and I is the current in amperes. The first three terms of each of these expansions were evaluated for $\rho = 0.0953$ meters, the mean radius of the beam, and R = 0.169 meters, the mean radius of the windings. The error in neglecting the rest of the terms and in using the mean radius of the winding is less than 0.1 percent for both the radial and axial components. The field due to the shaping coil was calculated by first determining the field due to a single loop using the formula given in Smythe.[29] Curves were plotted for both the axial and radial components and graphically integrated over the external coil length.

The magnetic field was measured experimentally by probing with a proton resonant device. The radio frequency coil and proton sample were fixed at the beam radius, but the azimuthal angle and the axial position could be varied. The experimental points shown in Figure 7 are an average of the values obtained at different azimuthal angles since the differences were less than 0.05 percent. The resonant frequency was determined by beating with a 500 kilocycle crystal oscillator, and measuring the beat frequency on a calibrated oscilloscope. All points were slightly below the field (1.1743×10^{-2} webers per square meter) corresponding to 500 kilocycles. The earth's magnetic field was cancelled by the earth correction coils except for the axial component of 1.6×10^{-5} webers per square meter which was opposed to the main solenoid field. This component of the earth's field was measured by reversing the solenoid field, measuring the field at a given point in the solenoid, subtracting this value from the value obtained with the normal field

direction, and taking one-half of the difference. Figure 7 shows the experimental points along with the calculated curve that fits the points best. The value of current for the solenoid and field shaping coil corresponding to the calculated curve are I(solenoid) = 6.2718 amperes and I(shaping coil) = 0.01762 amperes. The corresponding radial component is shown in Figure 8. The calculated values are tabulated in Appendix II, Part A.

Trapping Duration

The time of flight between the two targets must also be determined accurately. The timing circuit generates accurately spaced pulses but the zero point, the actual injection time with respect to the generated pulses, has to be determined. By operating the counters as straight geiger counters (not pulsed) and by keeping the beam intensity low, both the initial pulses and the delayed pulses can be observed simultaneously on an oscilloscope. The initial pulses correspond to electrons with too much axial momentum to be trapped, and they indicate the true injection time. By monitoring both the delayed and initial pulses on a calibrated scope, the zero time was determined to be 0.6 $\pm$ 0.05 microseconds. This means that 0.6 microseconds should be subtracted from the times indicated on the timing circuit, and in the graphs indicating trapping time to obtain the true trapping time. The zero time can also be determined by a statistical analysis of the difference frequency curves for a number of different trapping times. This method will be treated in more detail in the next chapter.

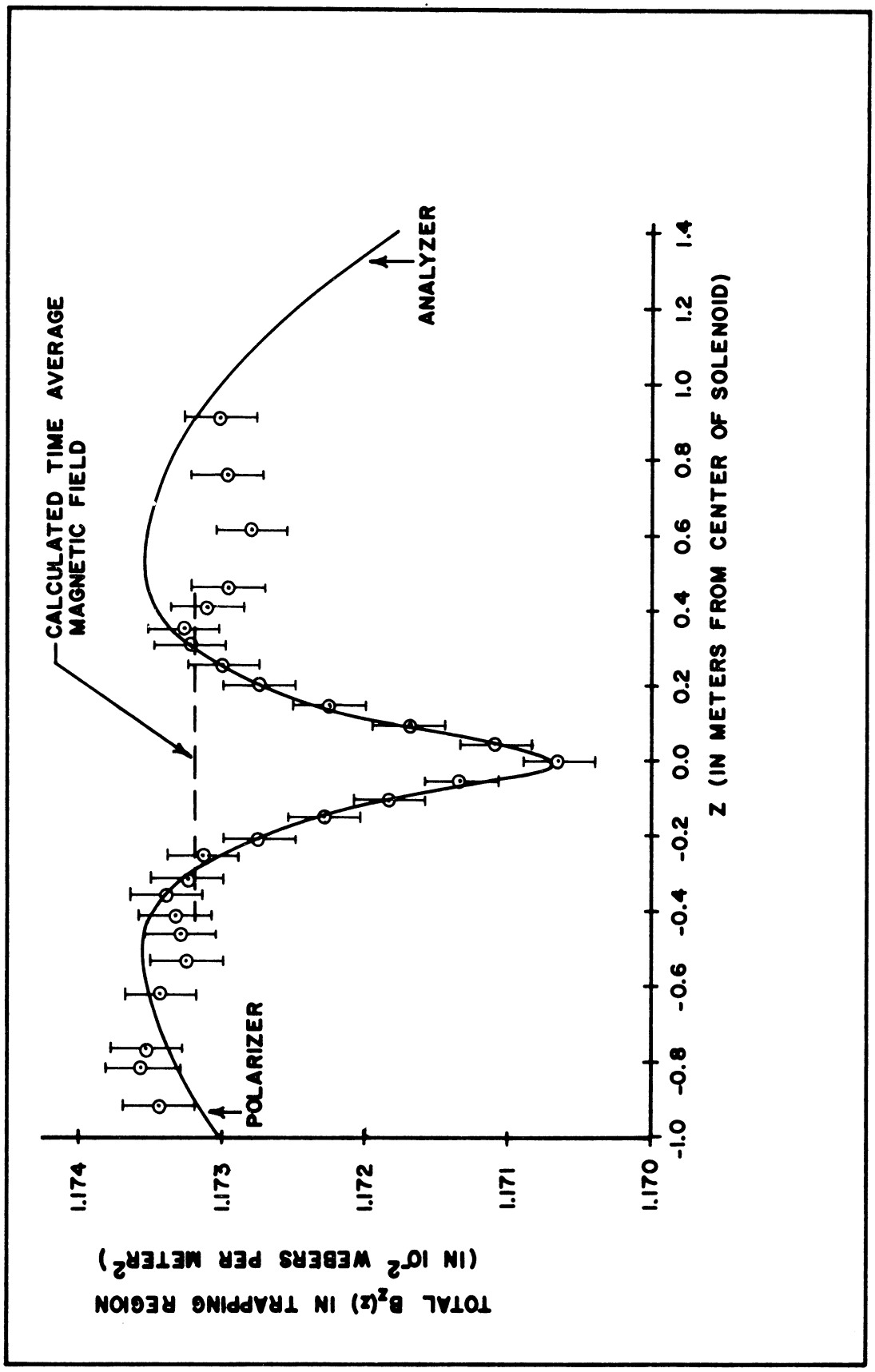

Figure 7. Axial Magnetic Field

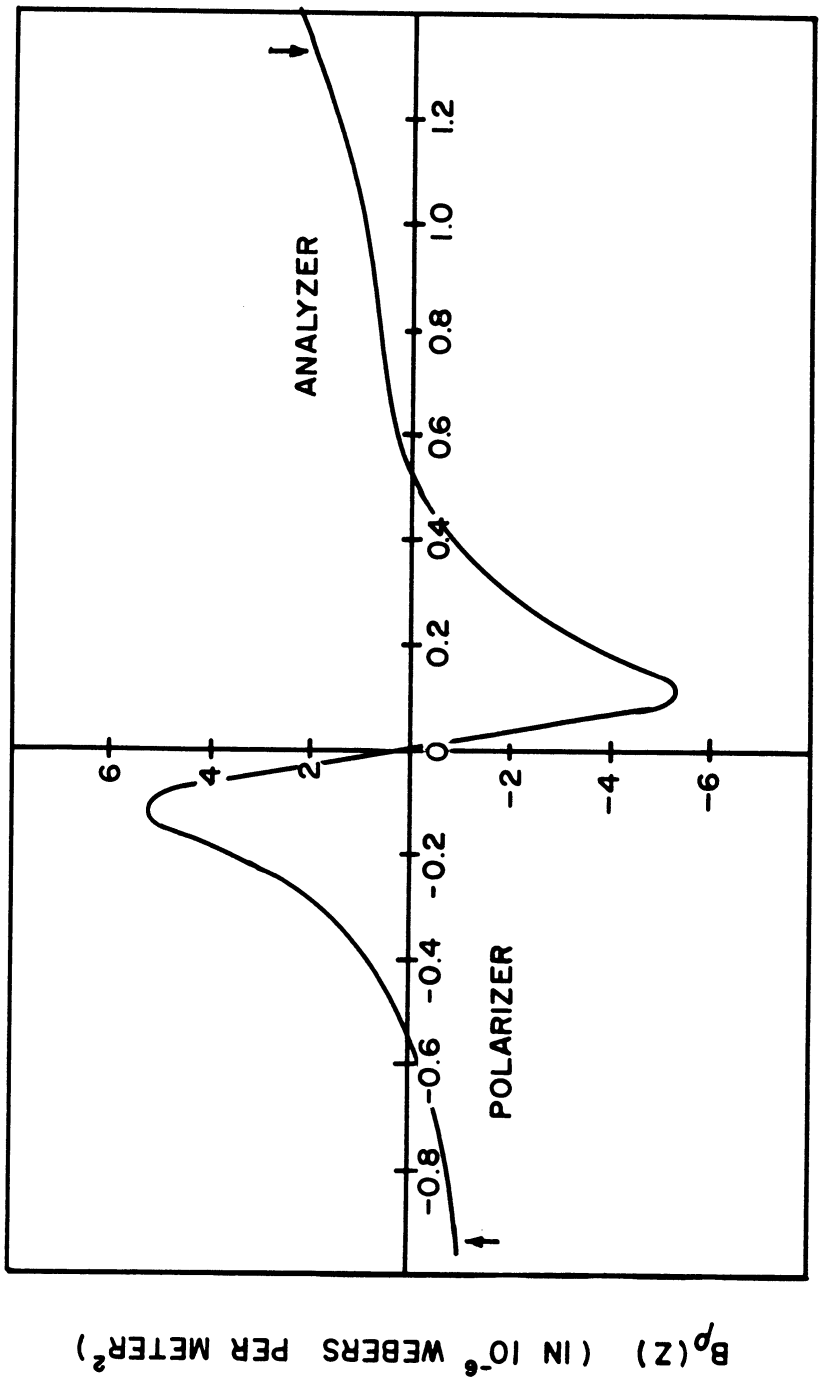

Figure 8. Radial Magnetic Field

Drift Frequency

The frequency with which the electrons oscillate in the shaped magnetic field is useful for calculating the average magnetic field and can be determined experimentally. For trapping durations up to about 35 microseconds the electrons remain bunched as they drift back and forth in the betatron field. This allows a measurement of the drift frequency by plotting the counting rate in either counter versus the trapping time, since more electrons will be ejected when the bunch is on the polarizer side of the gap than when it is on the analyzer side. The trapping time was varied in steps of 0.1 microseconds and the results are shown in Figure 9. The frequency determined from this graph is 1.14 megacycles which corresponds to a period of 0.88 microseconds.

Spurious Asymmetries

Spurious asymmetries may be present after second scattering even for the case of no Mott polarization of the beam. This is due to possible asymmetric scattering angles to the two counters, asymmetric magnetic fields, and misalignment in the slits, counters, and target holder.

The scattering angle for the two counters is different due to the fact that the beam travels in a helix and, therefore, strikes the analyzer target at a slight angle. The two counting rates are, therefore, different due to the angle dependence of the scattering cross section. The angle of incidence is not fixed in time since it depends on the axial momentum given the beam on ejection which, in turn, depends on the position of the beam in the trap and on the trapping time. By using an aluminum analyzer target the spurious instrumental asymmetries

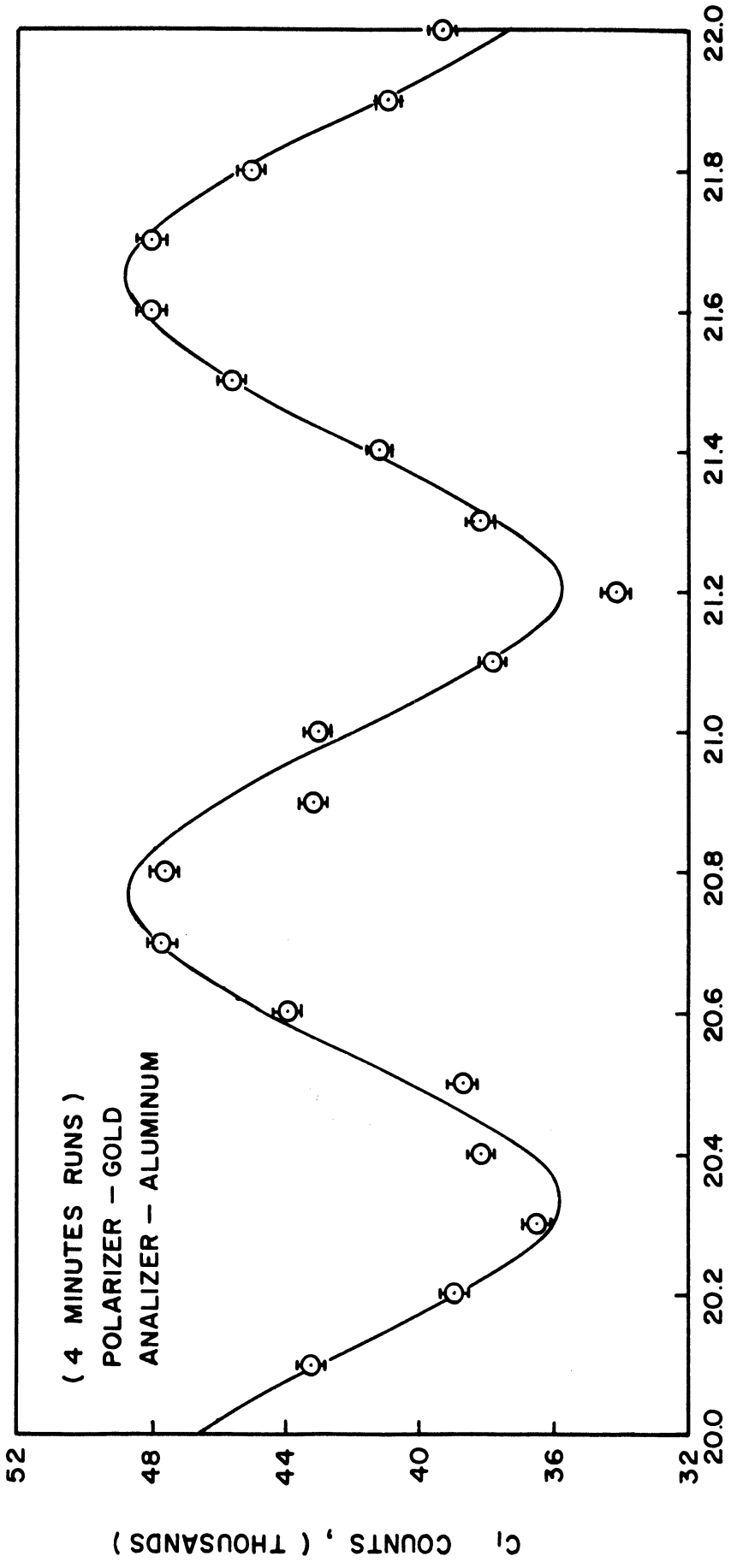

Figure 9. Drift Frequency

can be measured since the Mott polarization for low Z elements is very small and any observed asymmetry will be due to spurious sources. Graphs of the spurious asymmetries for trapping times from 30 to 300 microseconds are shown in Figures 10 to 12, and the raw data is tabulated in Appendix I, Part A. The spurious asymmetries are considerably smaller than the Mott asymmetry, both are shown in the 300.0 to 305.5 microsecond graph shown in Figure 12 for comparison, and were neglected in the final analysis for the difference frequency. The error flags shown are due to just the statistical fluctuations in the number of electrons counted.

Other spurious asymmetries can also arise from time variations in the high voltage used to accelerate the electrons, in the solenoid current, in the shaping coil current, and in the ejection pulse voltage. These asymmetries are much harder to evaluate and are minimized by highly regulating the above parameters. Graphs of the counting ratio for a gold polarizer and an aluminum analyzer target versus the solenoid current and high voltage are shown in Figure 13, and Figure 14 shows the counting ratio versus the shaping coil current and the ejection pulse voltage. The regulating range indicated in each graph is the maximum drift observed over a period of a few hours. From these graphs it can be seen that spurious asymmetries of this type are very small ($\sim 0.5\%$) and are negligible compared to the Mott asymmetry. Drifts of this type are slow compared to the time necessary to measure one section of the difference frequency (5.5 microsecond period of trapping time) and, thus, cause a slow level shift of the counting ratio with only a negligible effect on the difference frequency.

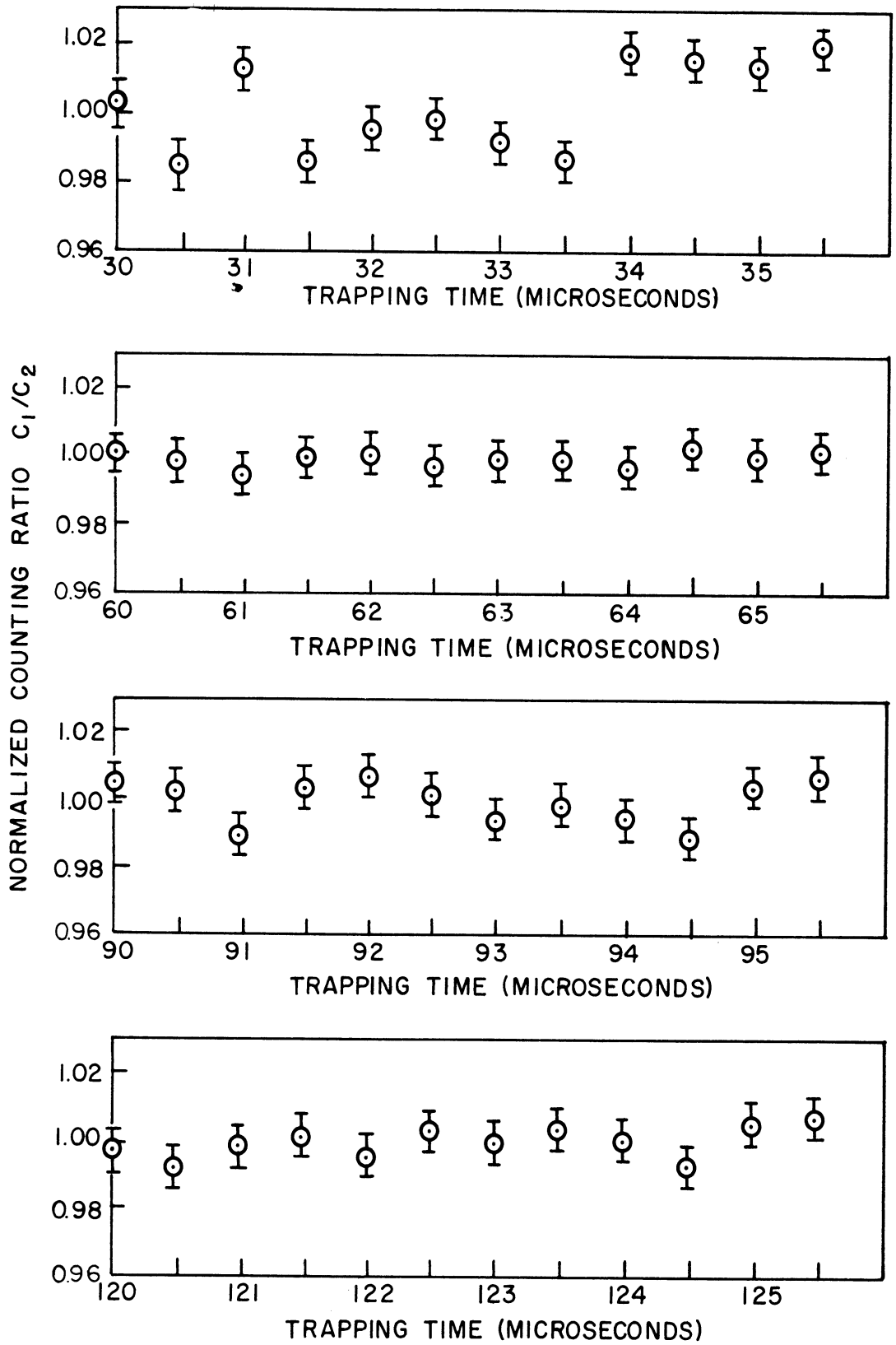

Figure 10. Spurious Asymmetries

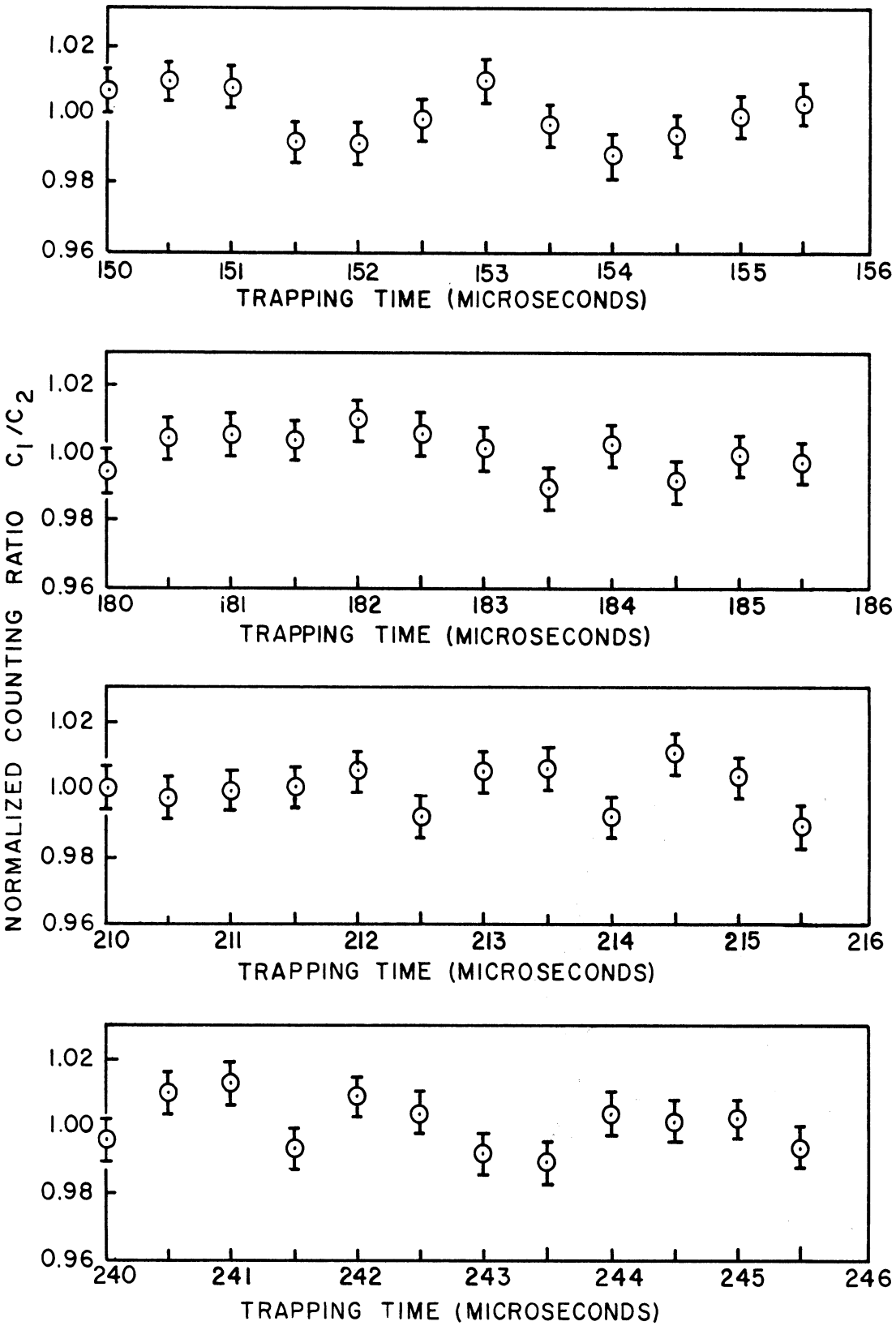

Figure 11. Spurious Asymmetries

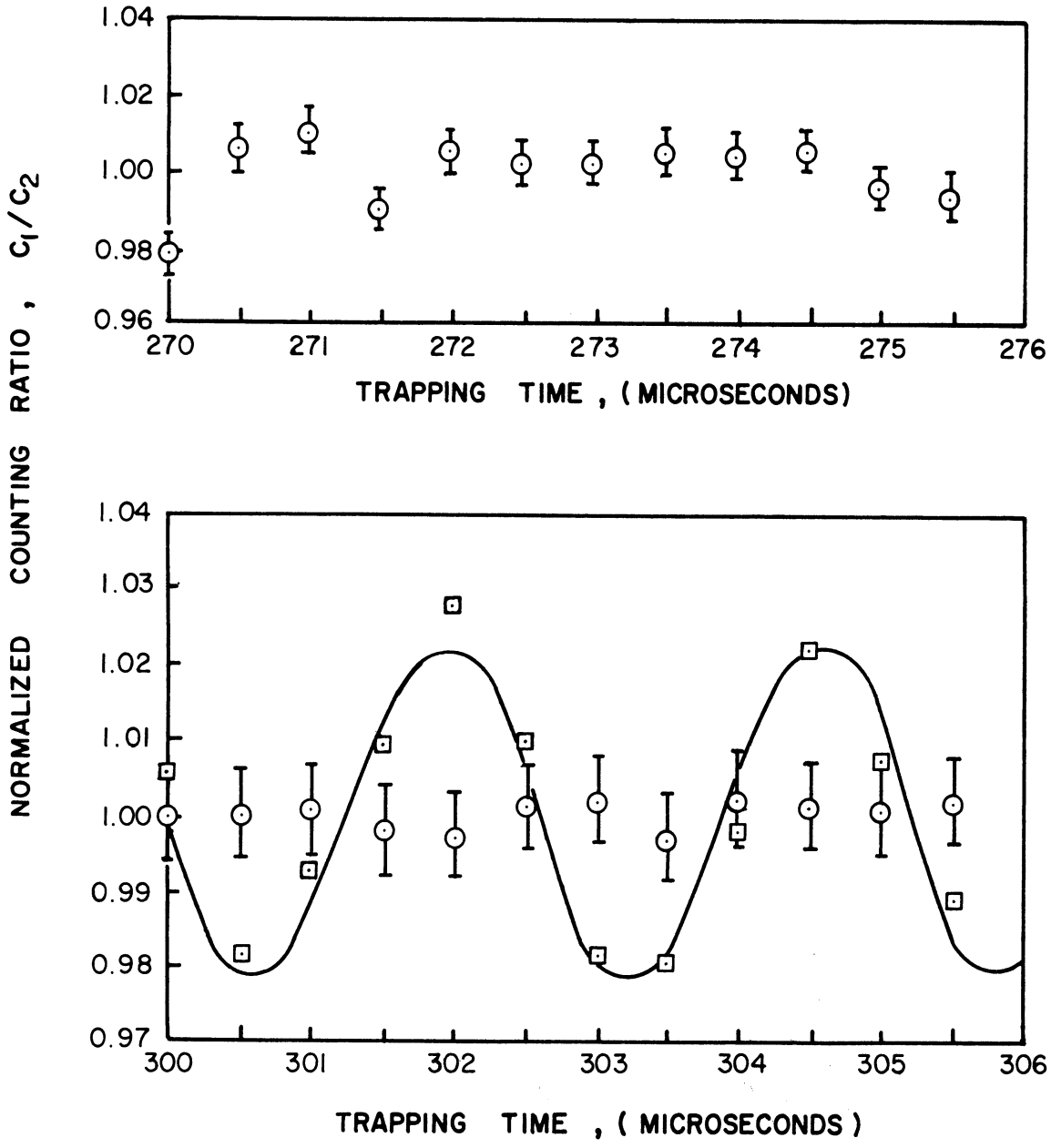

Figure 12. Spurious Asymmetries

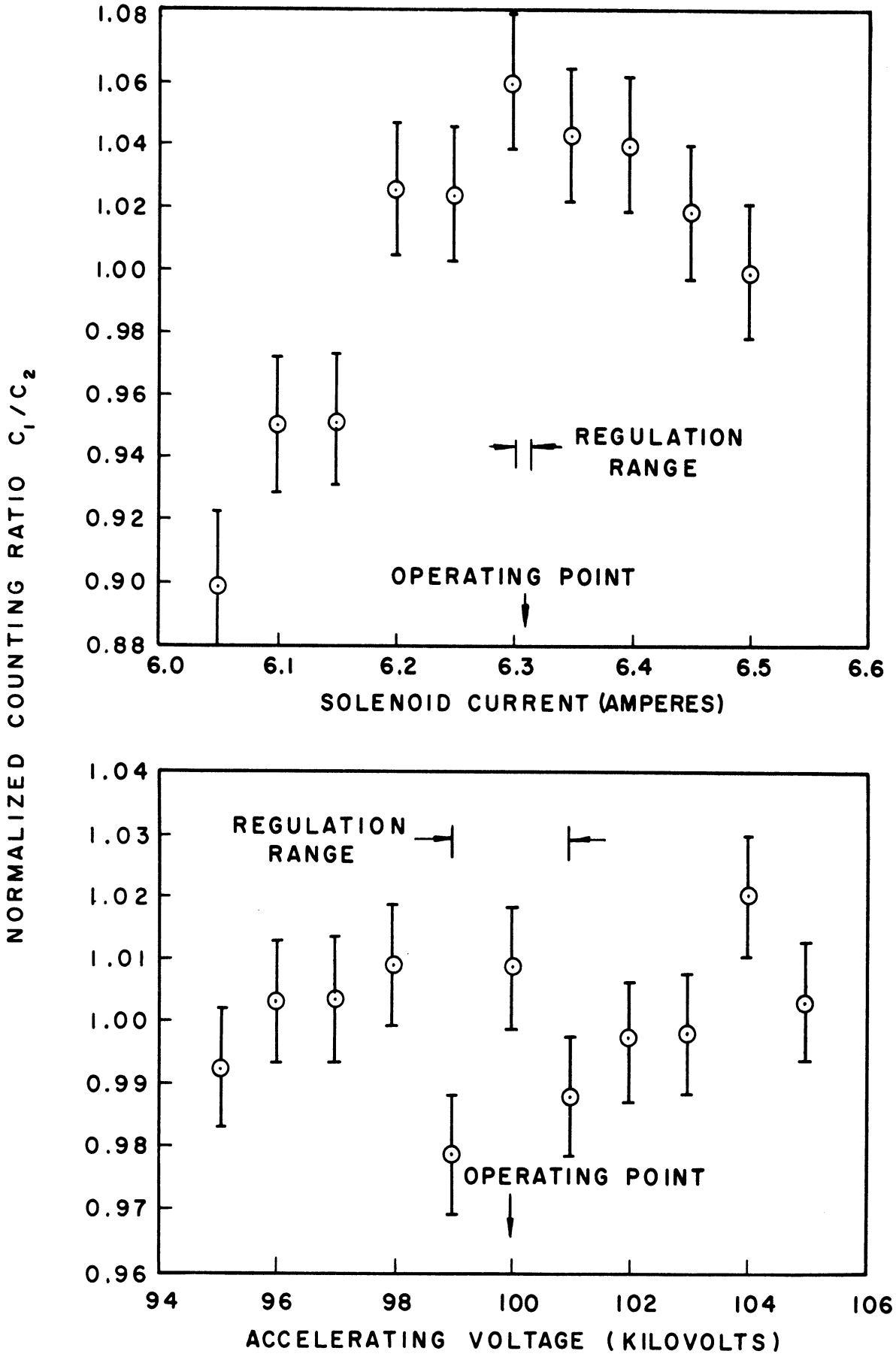

Figure 13. Spurious Asymmetries

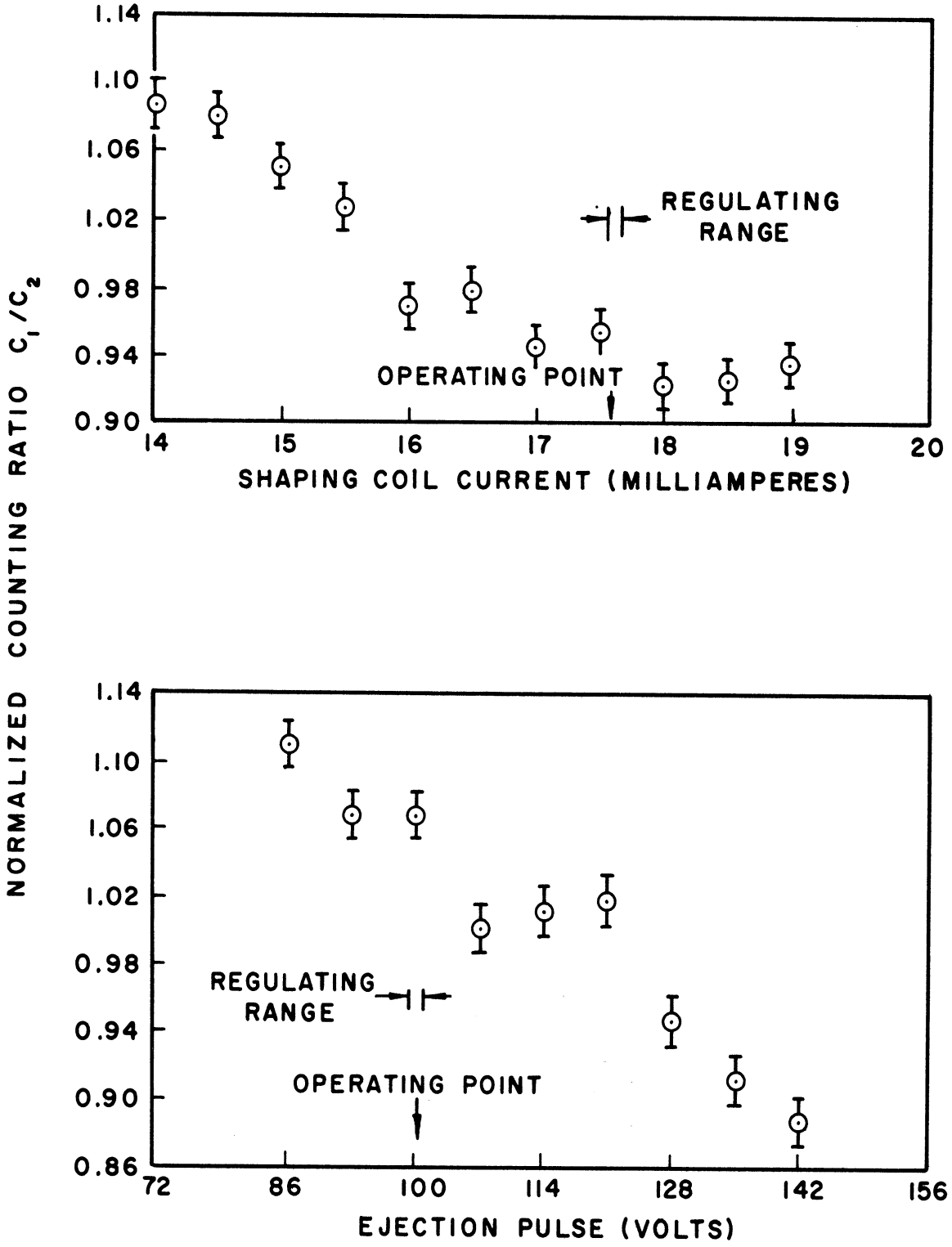

Figure 14. Spurious Asymmetries

IV. EXPERIMENTAL RESULTS AND ANALYSIS

Theory

The theory of double scattering was investigated by Mott[23] in 1929. Using the Dirac wave equation, he calculated the double scattering cross section of a beam of electrons. The basic assumptions for the calculation were an unpolarized initial beam that undergoes single elastic scattering by an atomic coulomb field. The results of this calculation show that there is an azimuthal asymmetry in the double scattering cross section given by

$$\sigma(\theta_1 \theta_2 \phi_2) = \sigma(\theta_1)\sigma(\theta_2)\left[1 + \delta(Z_1\theta_1 Z_2\theta_2)\cos\phi_2\right] \tag{4.1}$$

where $\sigma(\theta)$ is the single scattering cross section for an unpolarized beam, $\delta(Z_1\theta_1 Z_2\theta_2)$ is the Mott asymmetry factor, and ϕ_2 is the azimuthal angle about the second incident beam direction. This theory has been experimentally checked by Nelson[24] and excellent agreement is obtained for the energies and angles used in the present g-factor anomaly experiment. The addition of a magnetic field between the two scatterers is not included in this calculation.

Mendlowitz and Case[28] investigated the theory of double scattering with a uniform magnetic field interposed between the scatterers. The Dirac relativistic wave equation was used with the addition of a Pauli type term to account for the anomalous magnetic moment of the electron. This Hamiltonian was transformed to the Foldy-Wouthuysen representation where the spin and space dependence can be separated to a very high degree of accuracy. In this form, both the spin and spatial

motion of the particle can be easily predicted and were found to agree with the classical model of a charged spinning top with a magnetic moment precessing in the magnetic field. The spin precession frequency obtained for the case of a uniform magnetic field is

$$\vec{\omega}_s = -\omega_c\left[(1+\gamma a)\vec{b} - a(\gamma-1)\frac{\vec{v}\cdot\vec{b}}{v^2}\vec{v}\right] \tag{4.2}$$

where $\omega_c = eB/\gamma m_o$ is the cyclotron frequency, a is the g-factor anomaly defined in terms of the magnetic moment by $\vec{\mu} = (1+a)e\hbar\vec{\sigma}/2m_o$, $\vec{b}$ is a unit vector in the magnetic field direction, and $\vec{v}$ is the electron velocity vector. For the particular case of the electron velocity perpendicular to the magnetic field between scatterers, the precession frequency reduces to

$$\vec{\omega}_s = (1+\gamma a)\vec{\omega}_c \tag{4.3}$$

where $\vec{\omega}_c$ is given by $-eB\vec{b}/\gamma m_o$ and $\gamma = (1 - v^2/c^2)^{-1/2}$. The difference frequency is defined by

$$\omega_D = |\vec{\omega}_s - \vec{\omega}_c| = |\gamma a\,\omega_c| = a\,\omega_o \tag{4.4}$$

where $\omega_o = eB/m_o$.

Case and Mendlowitz also showed, for this particular case, that the double scattering cross section is

$$\sigma(\theta_1\theta_2\phi_2) \sim 1 + \delta(Z_1\theta_1 Z_2\theta_2)\cos\phi_2\cos\epsilon \tag{4.5}$$

where $\epsilon = \gamma a \omega_c T = \omega_D T$, T is the time spent in the magnetic field, $\delta(\theta_1 Z_1 \theta_2 Z_2)$ is the Mott asymmetry factor, and ϕ_2 is the azimuthal angle. This equation shows that the double scattering asymmetry rotates at the difference frequency as the trapping time is changed. A measurement of this frequency and the magnetic field constitutes a direct measurement of the g-factor anomaly since

$$a = \omega_D/\omega_c = m_o \omega_D / eB \tag{4.6}$$

A more general expression for the spin precession has been obtained by Ford[30] using the Dirac wave equation with the addition of terms to account for the anomalous magnetic moment and for a possible electric dipole moment of the electron. The result is

$$\begin{aligned}\vec{\omega}_s = &-\frac{e}{\gamma m_o}\left[\vec{B} - \frac{\gamma}{\gamma+1}\frac{\vec{v}\times\vec{E}}{c^2}\right] \\ &-\frac{ea}{m_o}\left[\vec{B} - \frac{\gamma-1}{\gamma}\frac{\vec{B}\cdot\vec{v}}{v^2}\vec{v} - \frac{\vec{v}\times\vec{E}}{c^2}\right] \\ &-\frac{ef}{m_o c}\left[\vec{E} - \frac{\gamma-1}{\gamma}\frac{\vec{E}\cdot\vec{v}}{v^2} + \vec{v}\times\vec{B}\right]\end{aligned} \tag{4.7}$$

where f, defined in terms of the electric dipole moment vector, is

$$\vec{P} = f e\hbar\vec{\sigma}/2m_o c \tag{4.8}$$

and a, the anomalous g-factor defined in terms of the magnetic moment vector, is

$$\vec{\mu} = (1+a)e\hbar\vec{\sigma}/2m_o \tag{4.9}$$

$\overline{E}$ is an arbitrary macroscopic electric field, and $\overline{B}$ is an arbitrary macroscopic magnetic field. This expression will be applied to the results of this experiment in a following section of this chapter.

Procedure for Measuring the g-Factor Anomaly

A measurement of the g-factor anomaly requires measuring both the difference frequency and the magnetic field. The difference frequency is obtained by measuring the counting rate ratio after double scattering as a function of trapping time. Thus, four experimental numbers are obtained, the two counting rates, the trapping time, and the magnetic field.

The counting rate in either counter may be expressed by

$$\eta = I(t)(N_{Z_1} d_{Z_1} \Delta\Omega_1)(N_{Z_2} d_{Z_2} \Delta\Omega_2)\epsilon\, \sigma_{Z_1}(\theta_1)\sigma_{Z_2}(\theta_2) \times \left[1 + \delta(Z_1\theta_1 Z_2\theta_2)\cos\phi_2 \cos\omega_D T\right] A(T) \tag{4.10}$$

where $I(t)$ is the initial beam intensity which may depend on the time, N_Z is the number of atoms per unit volume in the target, d_Z is the effective target thickness, $\Delta\Omega$ is the solid angle, ϵ is the counting system efficiency, $\sigma(\theta)$ is the single scattering cross section $\delta(Z_1\theta_1 Z_2\theta_2)$ is the Mott asymmetry factor, and $A(T)$ is the spurious instrumental asymmetry which may depend on the trapping time. The ratio of the counting rates in the two counters C_1 and C_2, see Figure 1, is now given by

$$\frac{\eta_1}{\eta_2} = C\frac{A_1(T)}{A_2(T)}\,\frac{1+\delta(Z_1\theta_1 Z_2\theta_2)\cos\phi_{21}\cos\omega_D T}{1+\delta(Z_1\theta_1 Z_2\theta_2)\cos\phi_{22}\cos\omega_D T} \tag{4.11}$$

The factor C is a constant with respect to the trapping time and the ratio of the spurious instrumental asymmetries is negligible compared to the Mott asymmetry as shown in Chapter III. Since the Mott asymmetry factor is small compared to unity, this expression (4.11) may be

simplified by expanding to first order with the following result

$$\frac{n_1}{n_2} = C\,\frac{A_1(T)}{A_2(T)}\left[1+\delta(\theta_1 Z_1 \theta_2 Z_2)\cos\omega_D T\left\{\cos\phi_{21}-\cos\phi_{22}\right\}\right] \qquad (4.12)$$

The angles ϕ_{21} and ϕ_{22} are fixed at $\phi_{21} = 19°$, and $\phi_{22} = 161°$ for this experiment so that the normalized counting ratio becomes

$$\frac{n_1}{n_2} = 1 + 1.9\,\delta(\theta_1 Z_1 \theta_2 Z_2)\cos\omega_D T \qquad (4.13)$$

The counting rate ratio was measured for various trapping times and energies. The trapping time was varied in steps of 0.5 microseconds over the range of 30 to 300 microseconds. Twenty-five groups of twelve points (5.5 microseconds) were taken and the raw data are tabulated in Appendix II, Part B. The magnetic field, shown in the tables as the voltage across the solenoid shunt, was varied with the energy to keep the beam radius fixed. The phase of each of these curves was determined by fitting a cosine by the method of least squares. An IBM 650 digital computer was used to determine the phase and the results of this calculation are shown in Table I. The phase indicated in Table I is the time corresponding to the maximum of the cosine curve.

The difference frequency is found by determining the number of cycles of a single cosine curve between zero trapping time and the phase point indicated in Table I. The period is given by

$$T_i = \frac{M_i - t_o}{N_i} \qquad (4.14)$$

where M_i is the time corresponding to the maximum of the i^{th} run, t_o is the time corresponding to zero trapping time ($t_o = 0.6 \pm 0.05$

TABLE I

PHASE OF THE DOUBLE SCATTERING ASYMMETRY RUNS

Run Number	Phase	Run Number	Phase
I	32.030	XIV	300.346
II	60.822	XV	302.657
III	92.307	XVI	203.042
IV	121.128	XVII	252.321
V	152.507	XVIII	268.062
VI	181.164	XIX	281.120
VII	210.189	XX	302.003
VIII	241.346	XXI	252.236
IX	270.422	XXII	301.776
X	301.703	XXIII	301.745
XI	301.941	XXIV	301.990
XII	301.913	XXV	303.266
XIII	301.961		

microseconds, as shown in Chapter III), and N_i is the number of cycles to the maximum of the i^{th} run. The errors in M_i and t_o are independent of the run number so the average period for a particular magnetic field is given by

$$T = \frac{\sum_i N_i^2 T_i}{\sum_i N_i^2} \tag{4.15}$$

The twenty-five runs are shown in Figures 15 through 23. The small arrows along the horizontal axis represent the maximum of the single cosine curve with a period given by Equation (4.15). The effect of an error in counting the number of cycles is shown in the first group of curves for the highest magnetic field used. The arrows with a plus sign represent the maximum points of a cosine curve with $N_i = \bar{N}_i + 1$ where $\bar{N}_i$ is the number of cycles for the best fit cosine. The arrows with a minus sign have $N_i = \bar{N}_i - 1$. In this way the correct period, corresponding to $\bar{N}_i$, can easily be found. A continuous run from 30 to 130 microseconds was also taken and the number of cycles in this run counted. The raw data for this run are tabulated in Appendix I, Part C, and the points are plotted in Figure 24.

The time average magnetic field seen by the trapped electrons must also be calculated. The axial force on the electrons is given by

$$F_z = e v_\phi B_\rho(z) = m \ddot{z} \tag{4.16}$$

where v_ϕ is the orbital velocity of the electrons and can be considered constant for this calculation since the magnetic field is essentially uniform and $B_\rho(z)$ is the radial magnetic field shown in Figure 8.

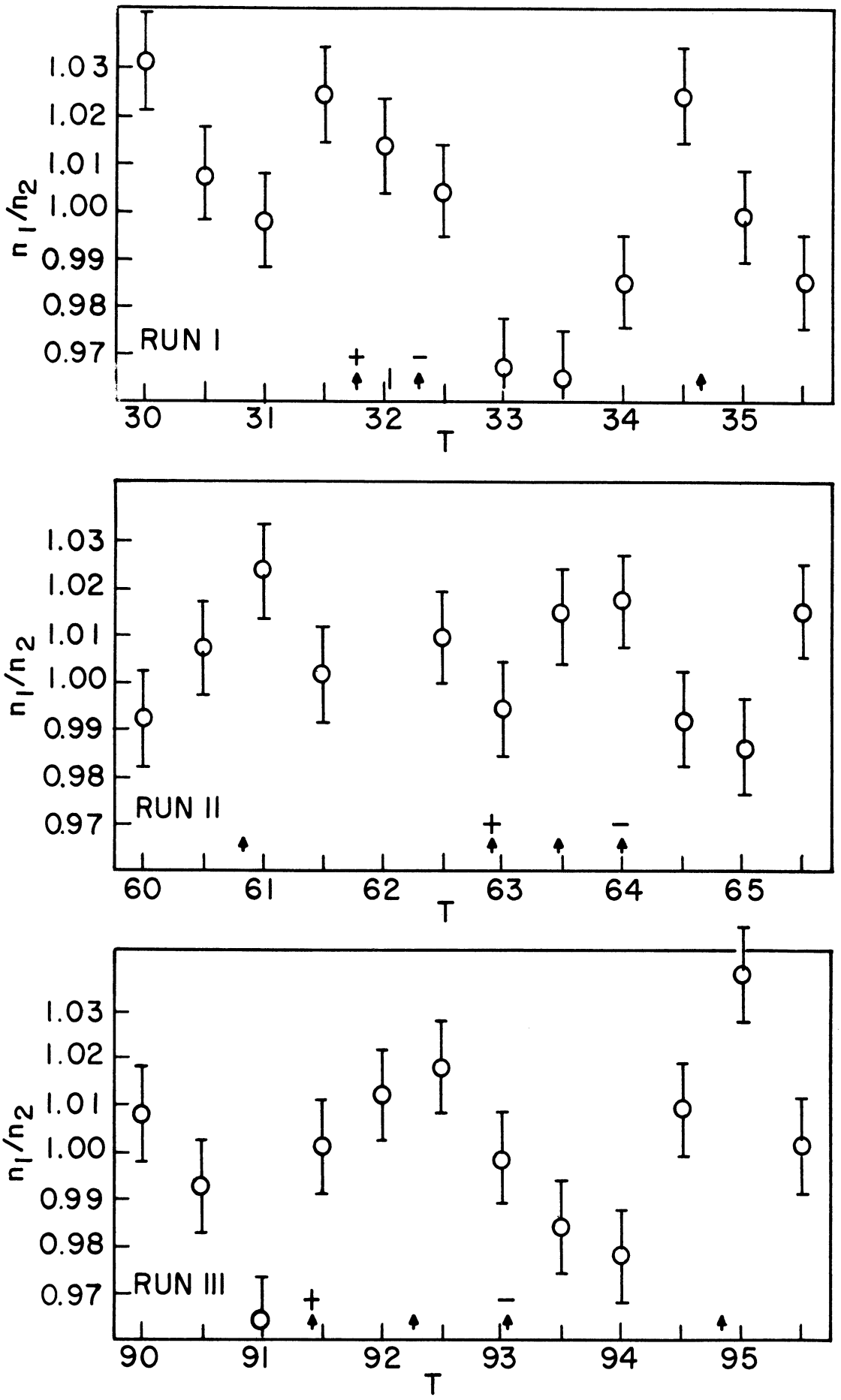

Figure 15. Double Scattering Asymmetry

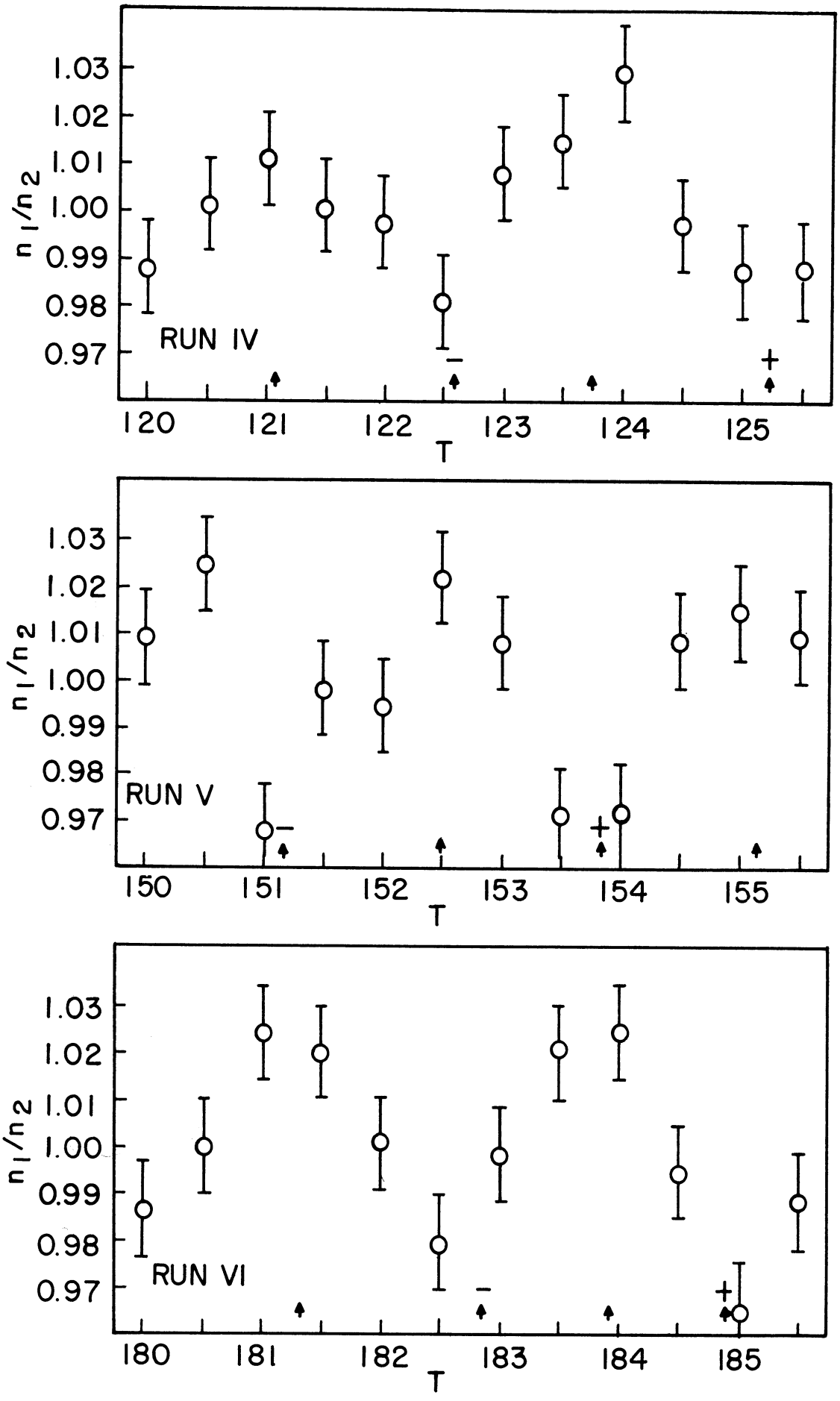

Figure 16. Double Scattering Asymmetry

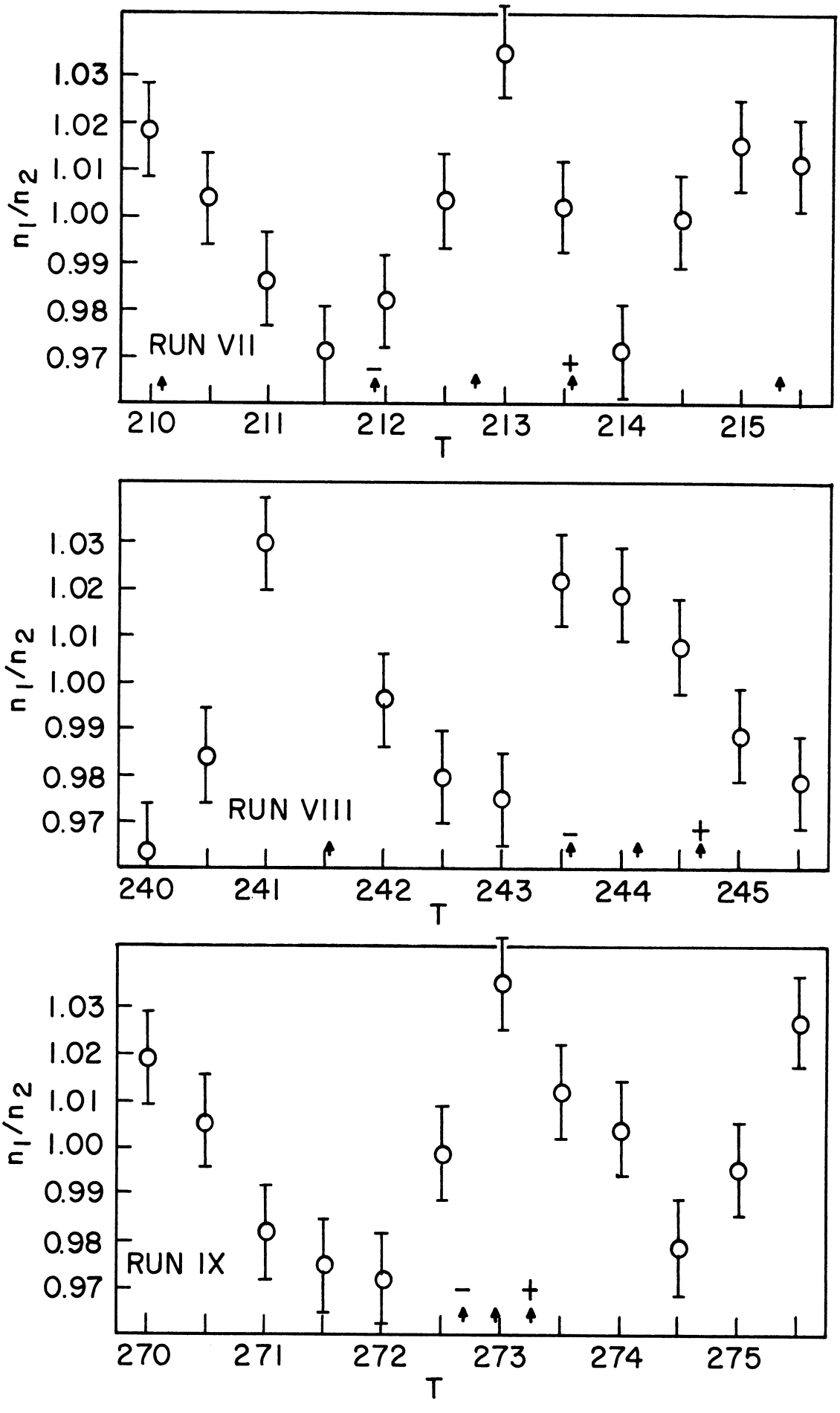

Figure 17. Double Scattering Asymmetry

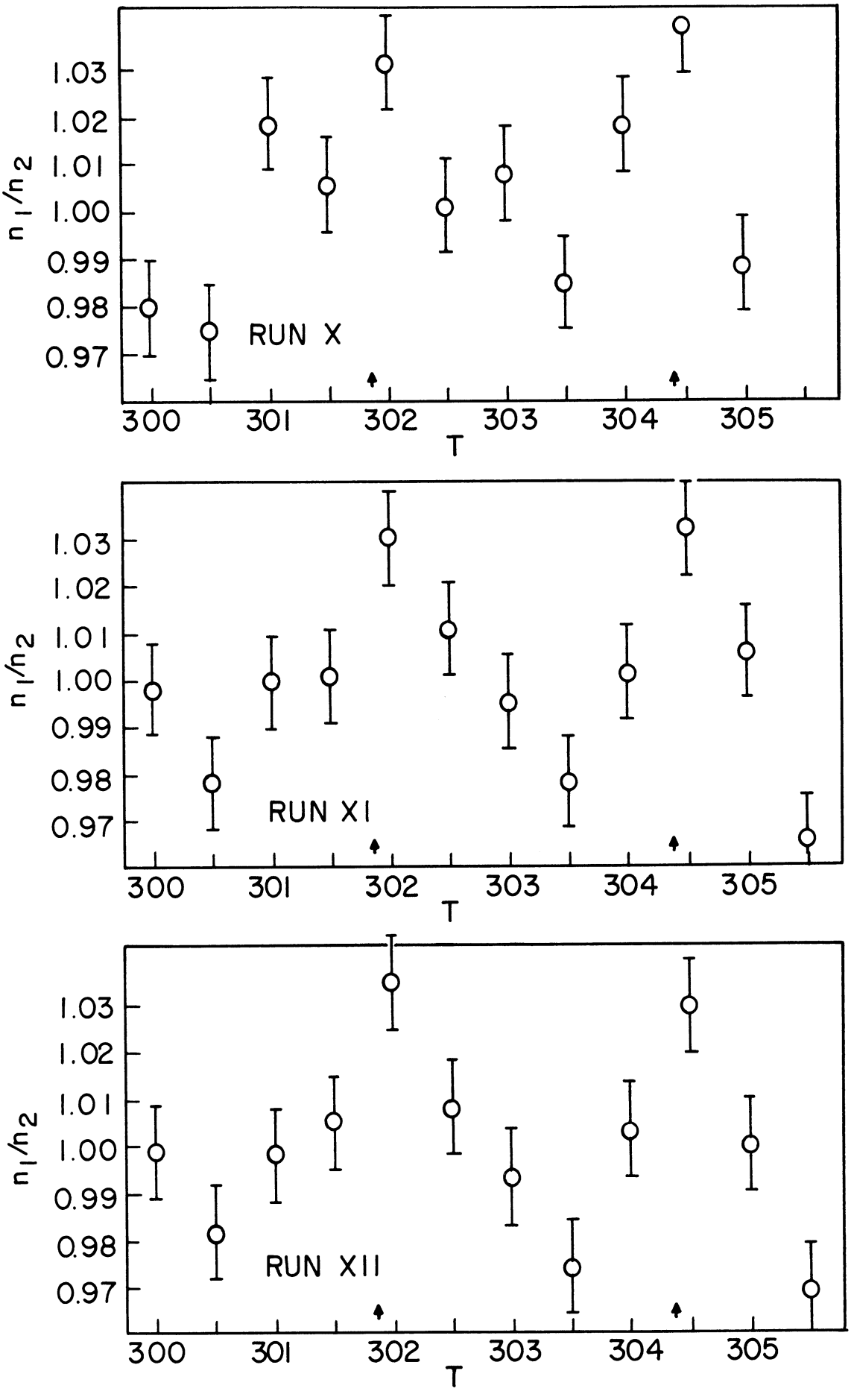

Figure 18. Double Scattering Asymmetry

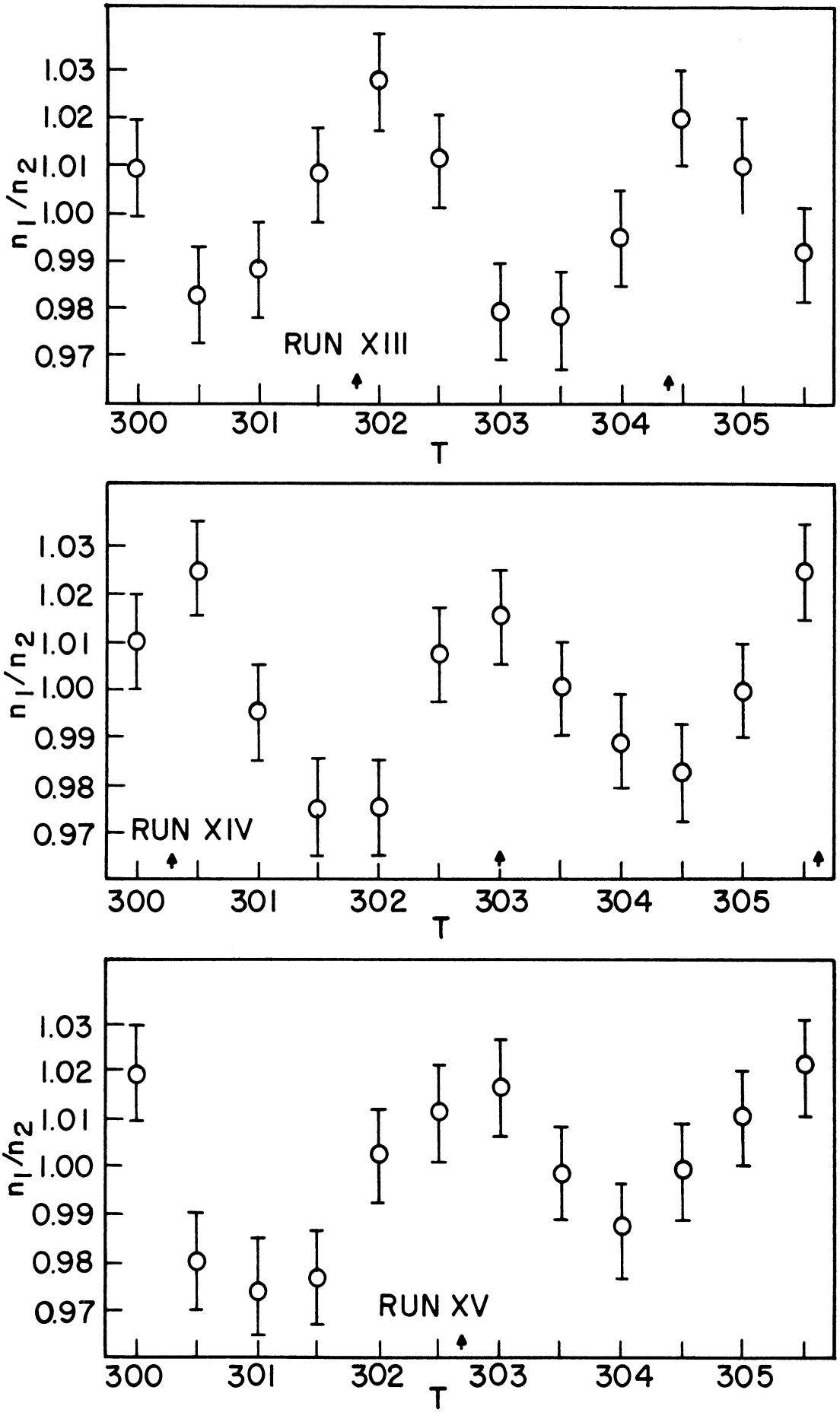

Figure 19. Double Scattering Asymmetry

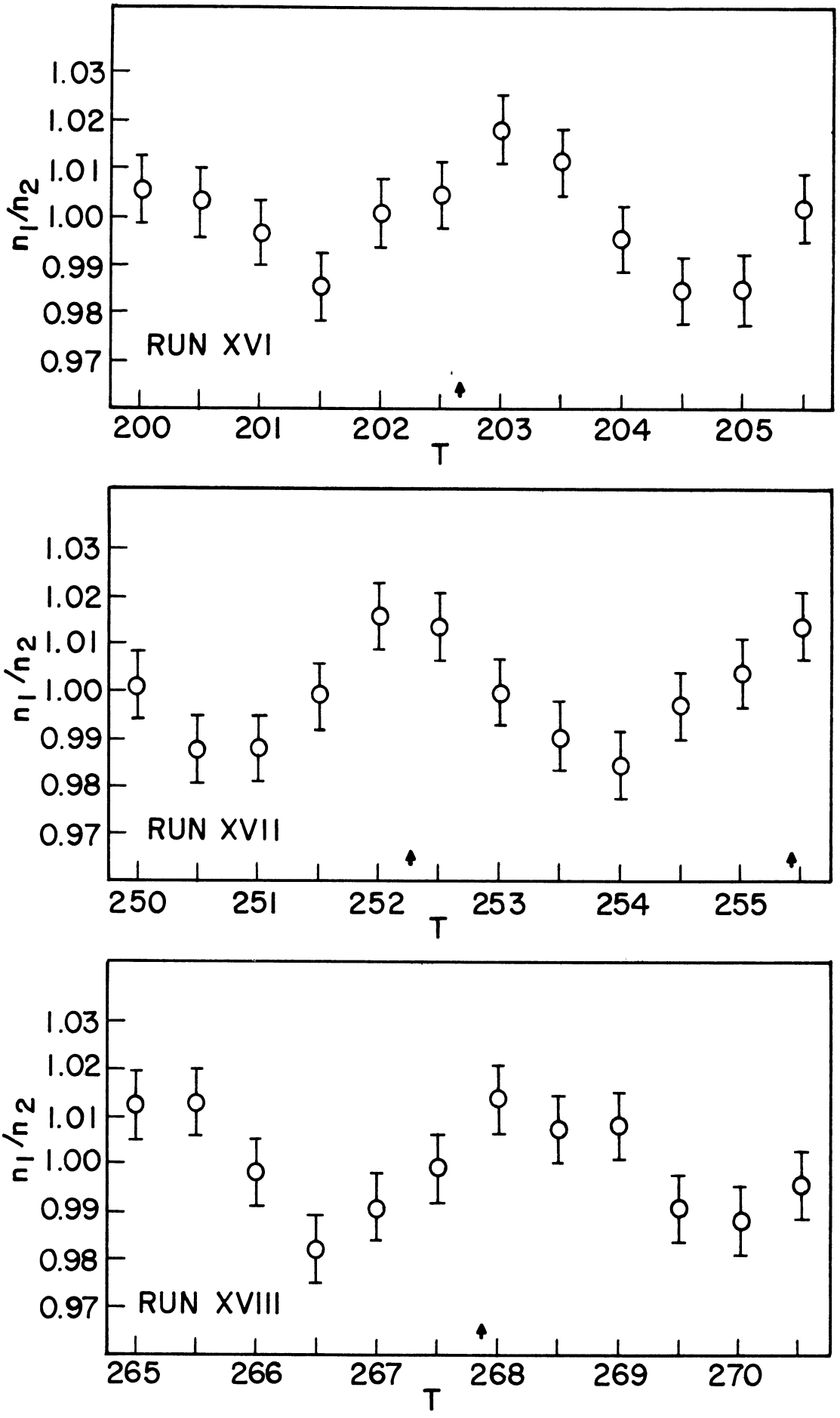

Figure 20. Double Scattering Asymmetry

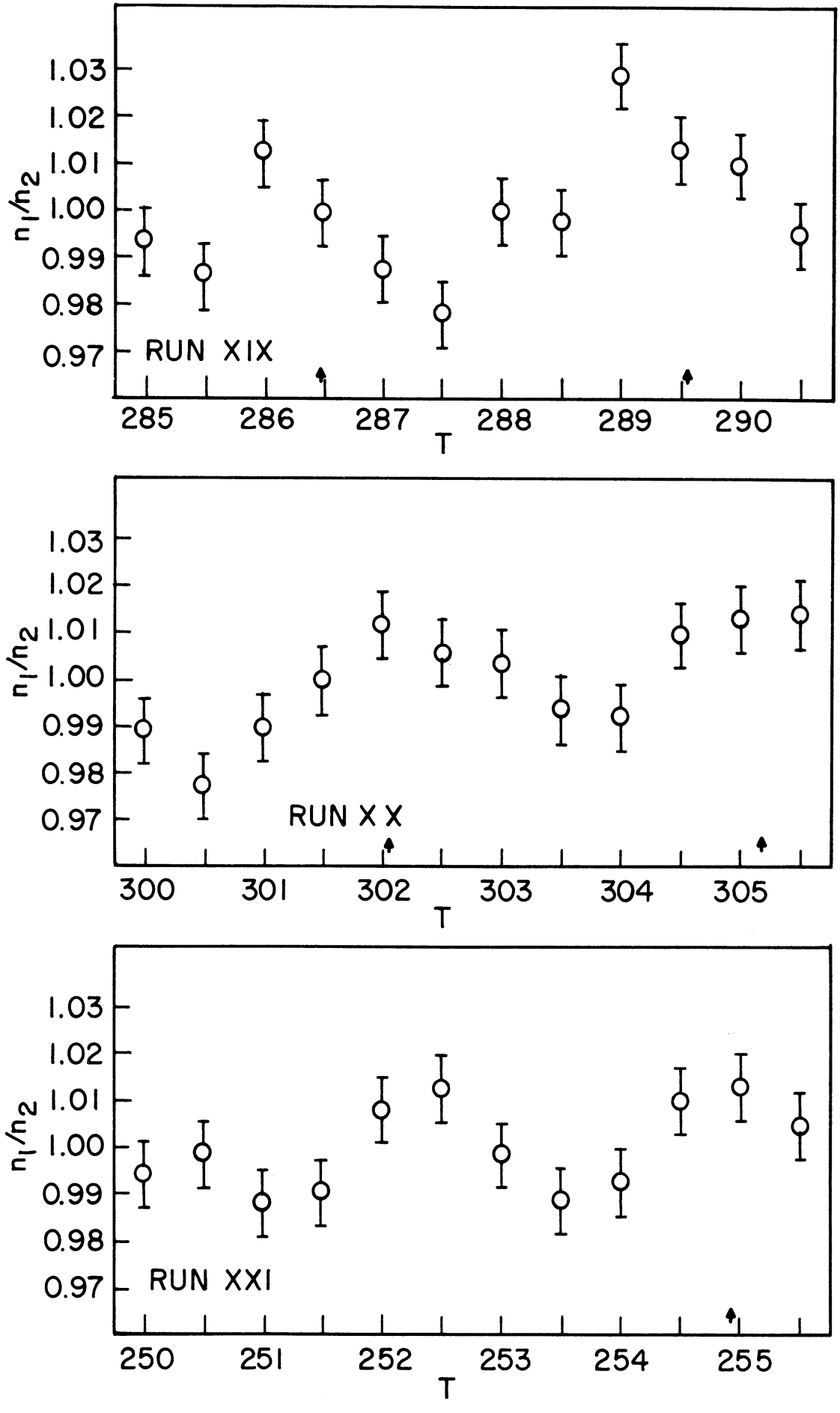

Figure 21. Double Scattering Asymmetry

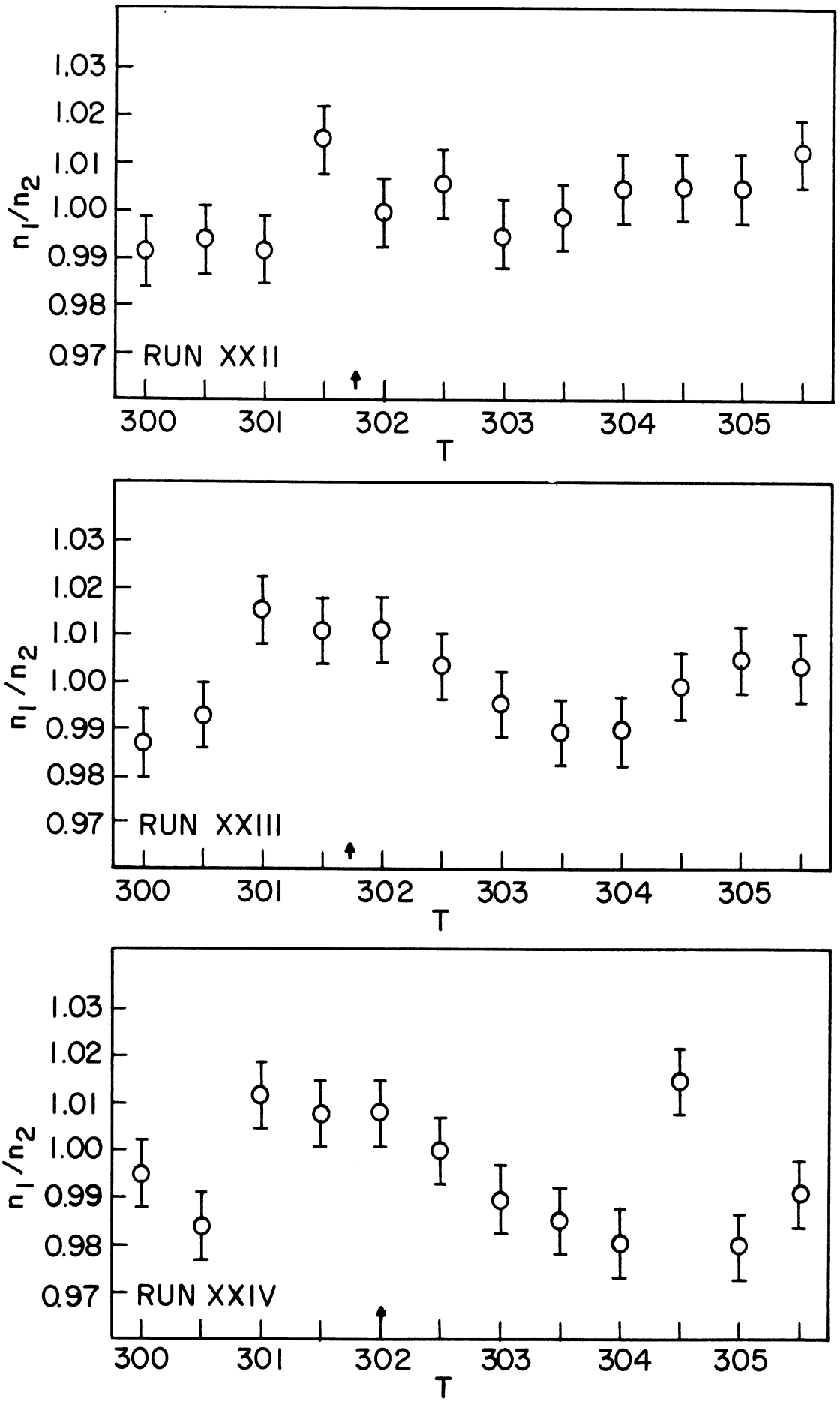

Figure 22. Double Scattering Asymmetry

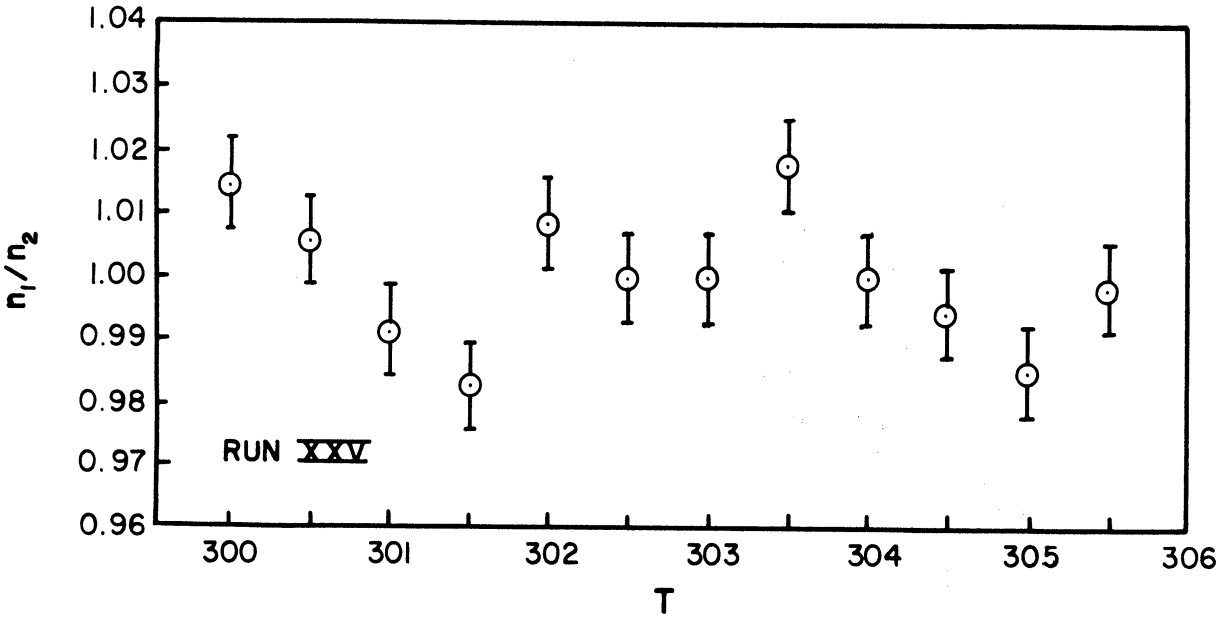

Figure 23. Double Scattering Asymmetry

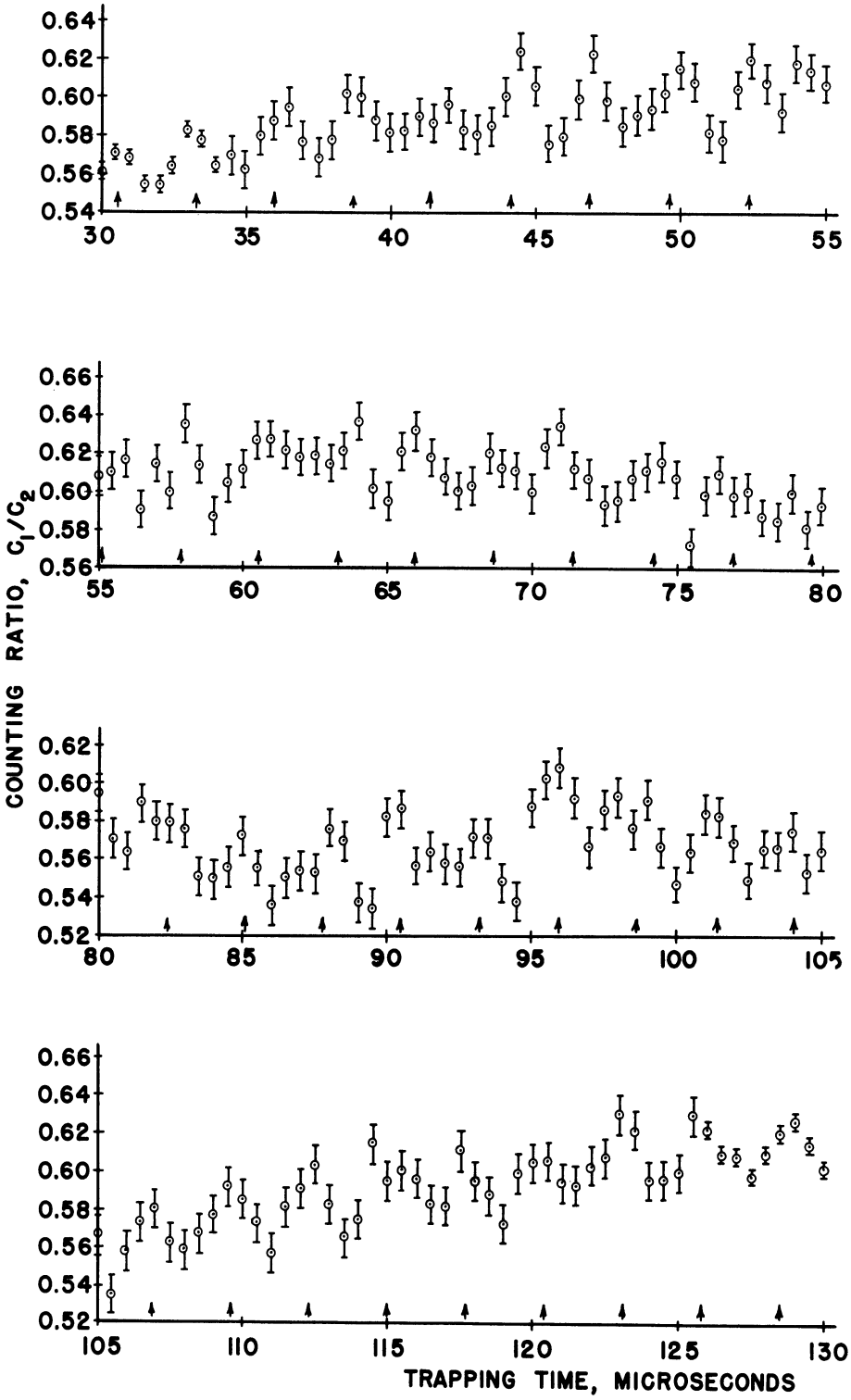

Figure 24. Double Scattering Asymmetry

Integrating Equation (4.16) once we obtain

$$\frac{1}{2}m(\dot{z})^2 = \int e V_\phi B_\rho(z)\,dz \tag{4.17}$$

The radial magnetic field was graphically integrated to give the effective axial potential well and the results are tabulated in Appendix II, Part B, and plotted in Figure 25. Solving Equation (4.17) for the time we obtain

$$t = \int \frac{dz}{\sqrt{\frac{2eV_\phi}{m}\int B_\rho(z)\,dz}} \tag{4.18}$$

Another graphical integration will then give the period of oscillation for electrons in the well. The axial velocity of the trapped electrons goes to zero on each side of the potential well so that the integrand of Equation (4.18) becomes infinite at these points. The graphical integration is good only from center of the well out to some finite distance from the point where the electron velocity goes to zero. Assuming the force over this small final interval to be constant, the time necessary for the electrons to travel this final interval is calculated by using

$$t = \sqrt{2mL/F} \tag{4.19}$$

where L is the length of the final interval and F is the average force over the interval. In this way the period of oscillation for trapped electrons with different amplitudes can be calculated. Figure 26 shows the results of this calculation. In Chapter III the measured period of oscillation was shown to be 0.88 microseconds, which corresponds to an amplitude of 0.487 meters. The time the electron spends in each interval

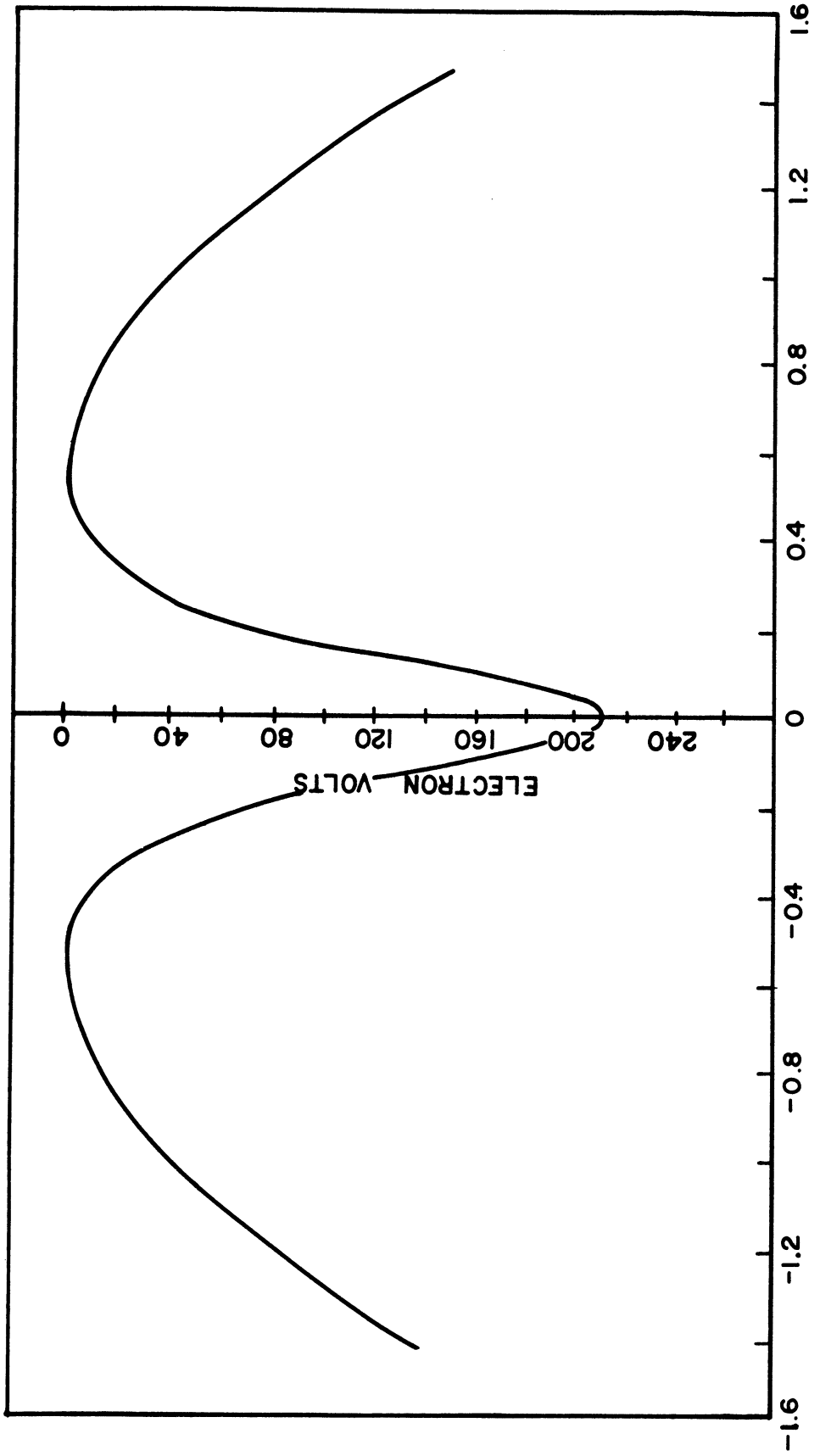

Figure 25. Effective Axial Potential Well

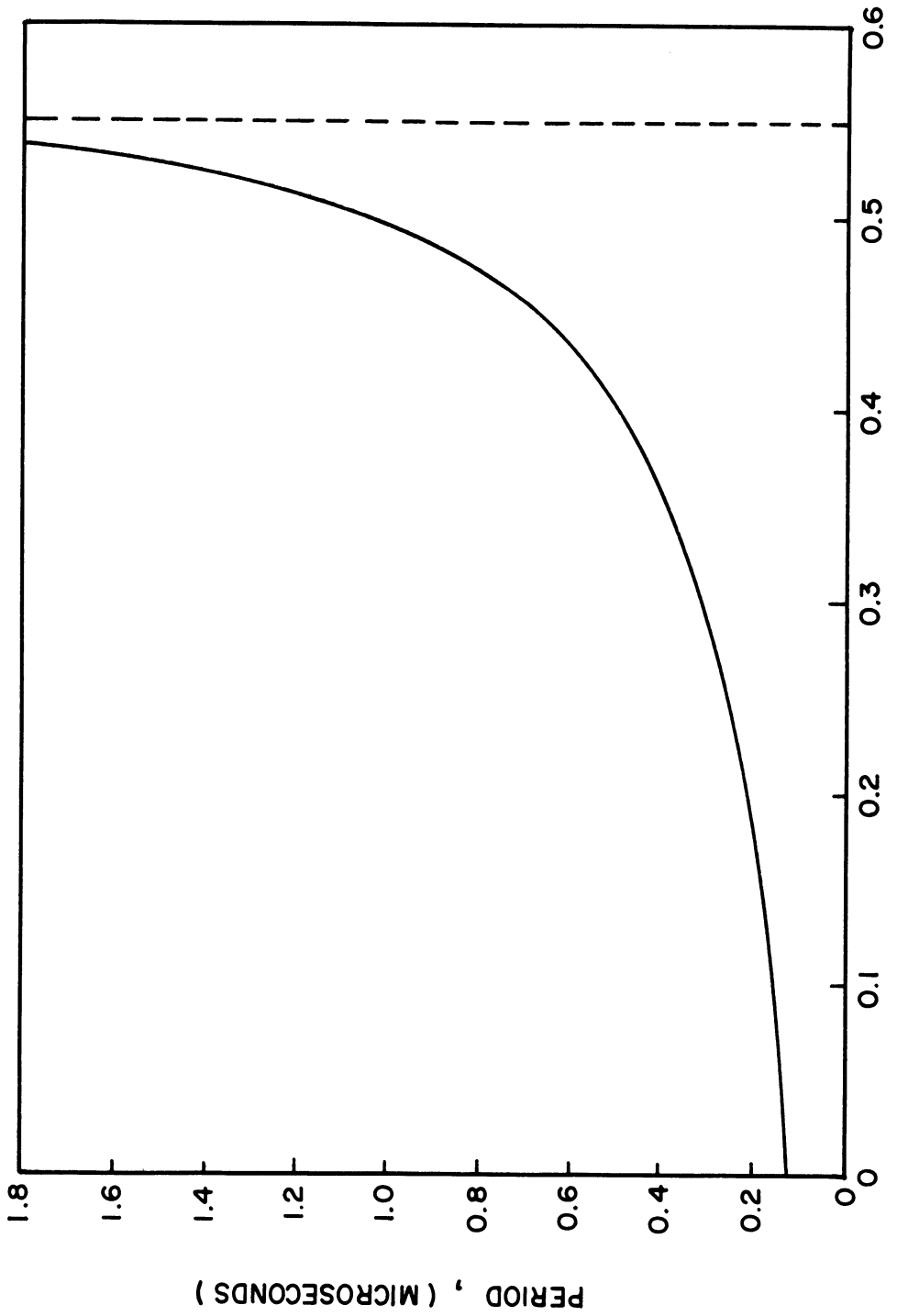

Figure 26. Oscillation Period in Well

Δz can be determined for this amplitude using the same procedure as used for the calculation of the oscillation period. The time average magnetic field can now be calculated using

$$B = \frac{1}{T} \sum_i B_i \Delta t_i \qquad (4.20)$$

where T is the period of oscillation (0.88 microseconds), B_i is the magnetic field in the i^{th} interval, and Δt_i is the time spent in the i^{th} interval. For a solenoid shunt reading of 0.8313 volts the calculated time average axial magnetic field seen by the trapped electrons is 0.0117319 webers per square meter. Since the earth's magnetic field has a component of 16×10^{-6} webers per square meter opposed to the solenoid field, the actual solenoid field corresponding to a shunt reading of 0.8313 volts is 0.117479 webers per square meter. Table II shows the time average magnetic field seen by the electrons for the different values of field used in measuring the double scattering asymmetry.

TABLE II

TIME AVERAGE MAGNETIC FIELD

Shunt Reading (Volts)	Time Average Magnetic Field	Shunt Reading (Volts)	Time Average Magnetic Field
0.5819	0.0082074	0.7500	0.0105830
0.6286	0.0088674	0.8000	0.0113056
0.6500	0.0091698	0.8212	0.0115892
0.7000	0.0098764	0.8313	0.0117319

The average values of ω_D/ω_o may now be calculated for the various values of energy and magnetic field used. The value for each measurement of the difference frequency period may be expressed by

$$(\omega_D/\omega_o)_j = 2\pi m_o/eBT_j = k/BT_j = kN_j/B(M_j - t_o) \tag{4.21}$$

where $k = 3.5712 \times 10^{-5}$ kilograms per coulomb, B is the magnetic field and T_j is the difference frequency period for the j^{th} run. The average value of ω_D/ω_o is given by

$$\overline{\omega_D/\omega_o} = \frac{\sum_j (\omega_D/\omega_o)_j \left(\frac{1}{s_j}\right)^2}{\sum_j \left(\frac{1}{s_j}\right)^2} \tag{4.22}$$

where s_j is the standard deviation for the measurement of $(\omega_D/\omega_o)_j$ and the sum is over all runs with the same magnetic field. Errors are present in the phase (M), the zero time (t_o), and in the magnetic field (B). These errors propagate into a standard deviation for the j^{th} run as follows

$$s_j = \frac{N_j k}{B^2(M_j - t_o)} \sqrt{(M_j - t_o)^2 s_B^2 + B^2(s_M^2 + s_{t_o}^2)} \tag{4.23}$$

where s_M is the standard deviation in the phase, s_{t_o} is the standard deviation in the zero time, and s_B is the standard deviation in the magnetic field. Table III shows the average value of ω_D/ω_o and the standard deviation for each magnetic field used. These values of ω_D/ω_o are plotted against $1/B^2$ as shown in Figure 27, and a straight line was fitted by the method of least squares. The intercept of this line at $1/B^2 = 0$ is $1.16064 \times 10^{-3} \pm 1.21 \times 10^{-6}$, and the slope is $2.309 \times 10^{-10} \pm 1.24 \times 10^{-10}$.

TABLE III

EXPERIMENTAL VALUES OF ω_D/ω_o

Magnetic Field (B)	$1/B^2$	Average ω_D/ω_o	Standard Deviation
0.0082074	1.48453×10^4	1.16448×10^{-3}	1.23695×10^{-6}
0.0088674	1.27177×10^4	1.16255×10^{-3}	1.22853×10^{-6}
0.0091698	1.18927×10^4	1.16308×10^{-3}	7.43456×10^{-7}
0.0098764	1.02519×10^4	1.16346×10^{-3}	6.15290×10^{-7}
0.0105830	0.89285×10^4	1.16224×10^{-3}	1.20615×10^{-6}
0.0115892	0.74455×10^4	1.16168×10^{-3}	1.19597×10^{-6}
0.0117319	0.72655×10^4	1.16232×10^{-3}	4.53150×10^{-7}

Interpretation of Results

According to Equation (4.6) the difference frequency divided by ω_o is equal to the g-factor anomaly and should be independent of the energy and magnetic field. Equation (4.6) assumes only an axial component of the magnetic field and an electron velocity exactly perpendicular to the magnetic field. The systematic shift of ω_D/ω_o versus $1/B^2$ shown in Figure 27 must be due to fields not included in this equation. A radial magnetic field is present in the system due to the shaped magnetic field and an axial electric field is present during the injection and ejection of the beam. Since the electrons are trapped in the magnetic well, the average axial force must be zero. This requires the average radial magnetic field to be zero as can be seen from Equation (4.16). Thus, the average precession of the magnetic moment vector of the electron

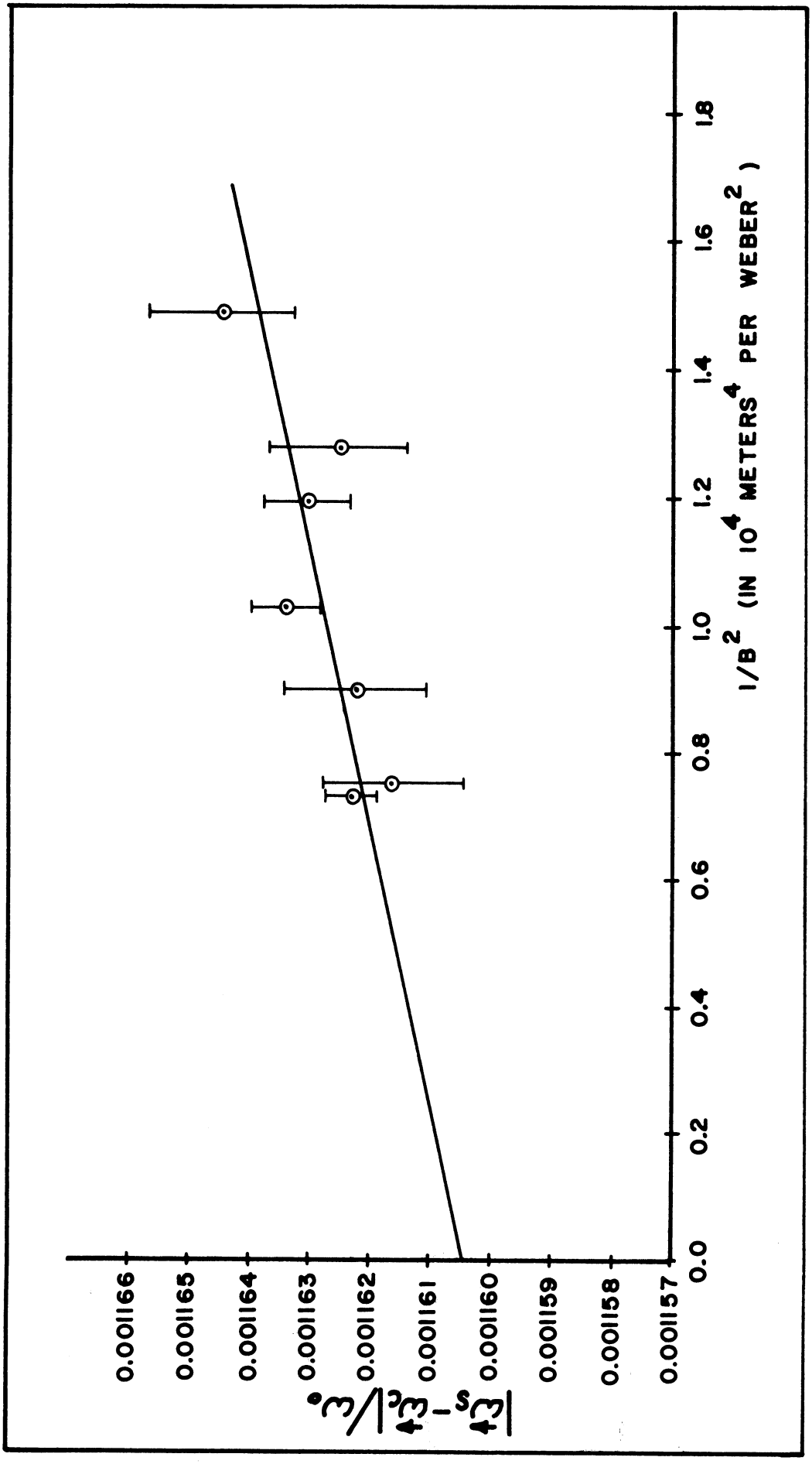

Figure 27. ω_D/ω_o Versus $1/B^2$ - Straight Line Fit

around the radial direction is also zero so that the radial component of the magnetic field will have negligible effect on the difference frequency and can be neglected. The axial electric field pulses also cause a precession of the magnetic moment vector about the radial direction due to the (v x E) term in Equation (4.7). These pulses are of the order of 200 volts per centimeter at the gap and are much smaller at the beam radius. An electron that is trapped will only pass this field once during injection and once during ejection, and the time spent in the field is approximately 10^{-8} seconds. This leads to a rotation of the spin vector of only about 10^{-2} radians. The rotations are in the opposite directions for injection and ejection since the electric pulse is reversed while the beam velocity (v_ϕ) remains unchanged. These two rotations tend to cancel each other, and the effect of the trapping pulses can be neglected in the measurement of the g-factor anomaly.

The systematic shift of the data must be due to other fields than the two mentioned above. Three other effects may be present, one due to the fact that the beam has a finite pitch as it drifts back and forth in the well, another due to any stray electric fields present in the trapping region due to charging of the surfaces of the concentric trapping cylinders and a third due to a possible electric dipole moment for the electron. Equation (4.7) is a general expression for the precession of the electron and includes the three effects just mentioned. Upon examination of the terms in (4.7), it is found that the effect of a radial electric field is at least 100 times greater than that due to an axial electric field or an azimuthal electric field. A radial electric field is also the most probable field present, due to the geometry of the

trapping system. The effect of the radial magnetic field was negligible and due to cylindrical symmetry, there is no azimuthal magnetic field. Specializing to the case of axial magnetic field and a radial electric field, Equation (4.7) becomes

$$\vec{\omega}_s = -\omega_o \left\{ \left[a + \frac{1}{\gamma} + (a + \frac{1}{\gamma+1}) \frac{vE}{Bc^2} \cos\alpha - a \frac{\gamma-1}{\gamma} \sin^2\alpha \right] \frac{\vec{z}}{z} \right.$$
$$- \left[(a + \frac{1}{\gamma+1}) \frac{vE}{Bc^2} \sin\alpha + a \frac{\gamma-1}{\gamma} \sin\alpha\cos\alpha \right] \frac{\vec{\phi}}{\phi} \qquad (4.24)$$
$$\left. + f \left[\frac{E}{cB} + \beta \cos\alpha \right] \right.$$

where α is the slight pitch angle of the helical trajectory of the beam and $\omega_o = eB/m_o$. The precession of the magnetic moment vector about the ϕ direction averages to zero over one complete cycle of the drift frequency since $\sin\alpha$ is an antisymmetric function of the motion. The only residual effect is due to one pass through the field from the first target to the second target. This precession amounts to only 0.001 radians when the values of the various trapping parameters are substituted into Equation (4.24) and can be neglected. One other term can be neglected. This is the term proportional to $\sin^2\alpha$ in the z component of the spin precession frequency. This term amounts to less than 0.1 percent of the g-factor anomaly, and since a 0.1 percent measurement is being made, this term is negligible. The cyclotron frequency for this type of motion is given by

$$\vec{\omega}_c = -\omega_o \left[\frac{1}{\gamma} + \frac{E}{\gamma B v \cos\alpha} \right] \frac{\vec{z}}{z} \qquad (4.25)$$

The difference frequency divided by ω_o is now obtained by subtracting Equation (4.25) from Equation (4.24), and then taking the absolute value of the resultant vector. This yields

$$\frac{\omega_D}{\omega_o} = \sqrt{\left[a + \frac{E}{cB}\left(\frac{\beta^2+1}{\beta}\right)\right]^2 + f^2\left[\frac{E}{cB} - \beta\right]^2} \qquad (4.26)$$

The $\cos\alpha$ factors have been made equal to unity since α is about 1° and the error introduced is negligible. Expression (4.26) contains three unknown quantities, 1) the g-factor anomaly a, 2) the electric dipole factor f, and 3) the stray electric field E. These quantities are evaluated by requiring this expression to pass through the weighted average of the experimental points shown in Figure 27, and have the same slope at this point as the straight line fitted by least squares.

Theoretically, the electron possesses no electric dipole moment and the experimental evidence[31] to date is in agreement with this prediction. If the electric dipole moment factor, f, is put to zero, Expression (4.26) reduces to

$$\frac{\omega_D}{\omega_o} = a + \frac{E}{cB}\left(\frac{\beta^2-1}{\beta} + a\beta\right) \qquad (4.27)$$

This expression is shown in Figure 28 and represents the best fit to the experimental points. In the limit as $\beta \to 1$, Expression (4.27) approaches the g-factor anomaly so that the intercept of the curve shown in Figure 28 gives the best experimental value of the anomalous g-factor. Using Equation(4.27), the g-factor anomaly, a, and the stray electric field can be found in terms of the weighted average of the experimental

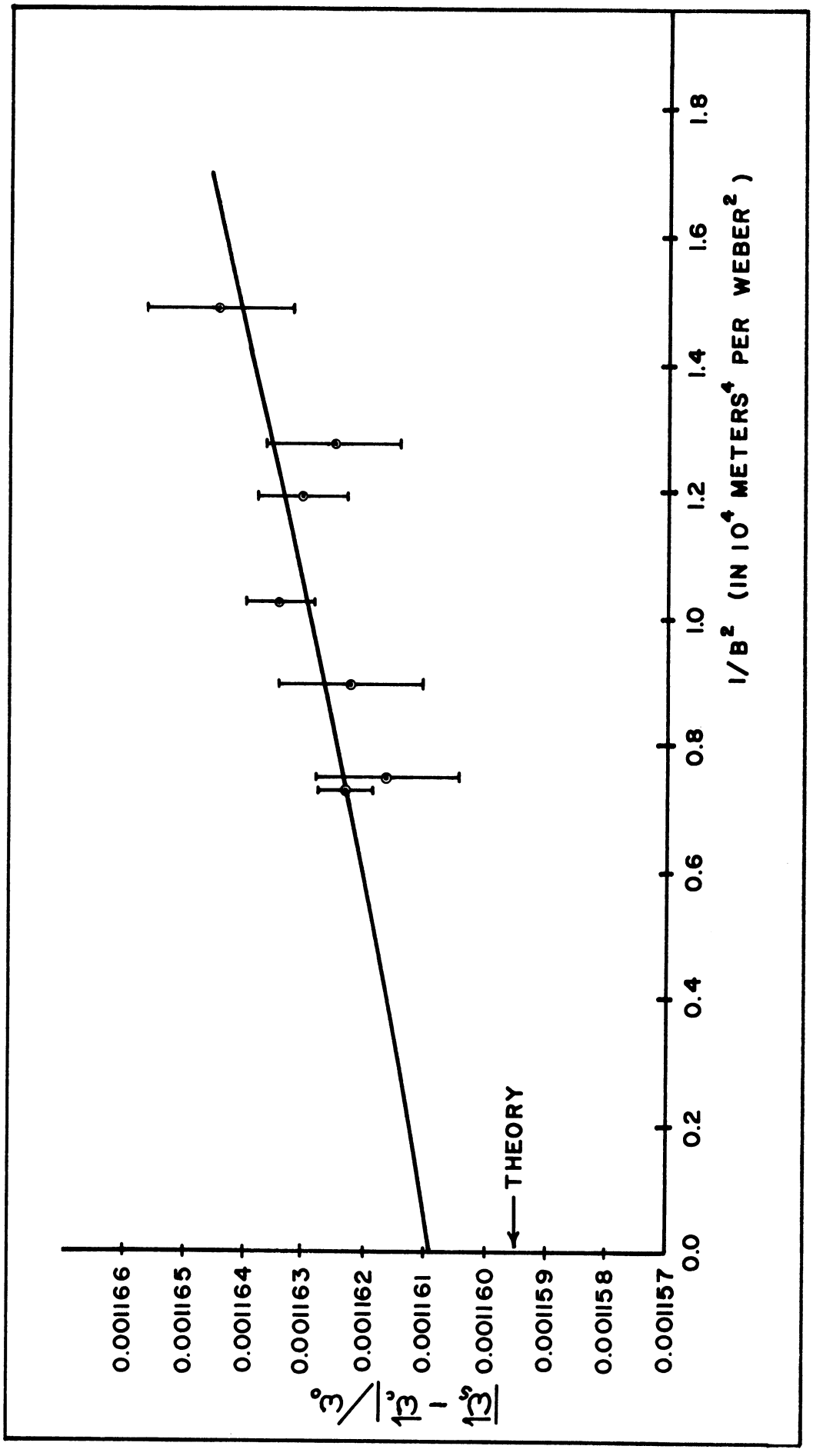

Figure 28. ω_D/ω_o Versus $1/B^2$ - Evaluation of "a"

points and the slope of the least square straight line. This calculation yields

$$a = \bar{N}_1 + ER/cB \qquad E = -cBN_2/F \tag{4.28}$$

where

$\bar{N}_1$ = weighted average of the experimental points

1.16278×10^{-3}

N_2 = slope of the least square straight line

2.309×10^{-10}

$R = 1/K \sqrt{K^2 + 1}$

$F = B^2R$

$K = e\rho B/m_o c$

ρ = beam radius of 0.953 meters

B = magnetic field at weighted average point

1.0389×10^{-2} webers per square meter.

Substitution of these values in (4.28) yields

a = 0.0011609 E = -4.0 volts per meter

The data may also be interpreted to yield information about the electric dipole moment of the electron by assuming the theoretical value of 0.0011596 for the g-factor anomaly of the electron. A plot of Expression (4.26) for this case is shown in Figure 29. The f-factor and the electric field for the best fit are given by

$$f = \sqrt{\frac{(\bar{N}_1 - a_T)F - N_2R}{IF + GR}} \qquad E = -\frac{cB(\bar{N}_1 - a_T)G + cBN_2I}{IF + GR} \tag{4.30}$$

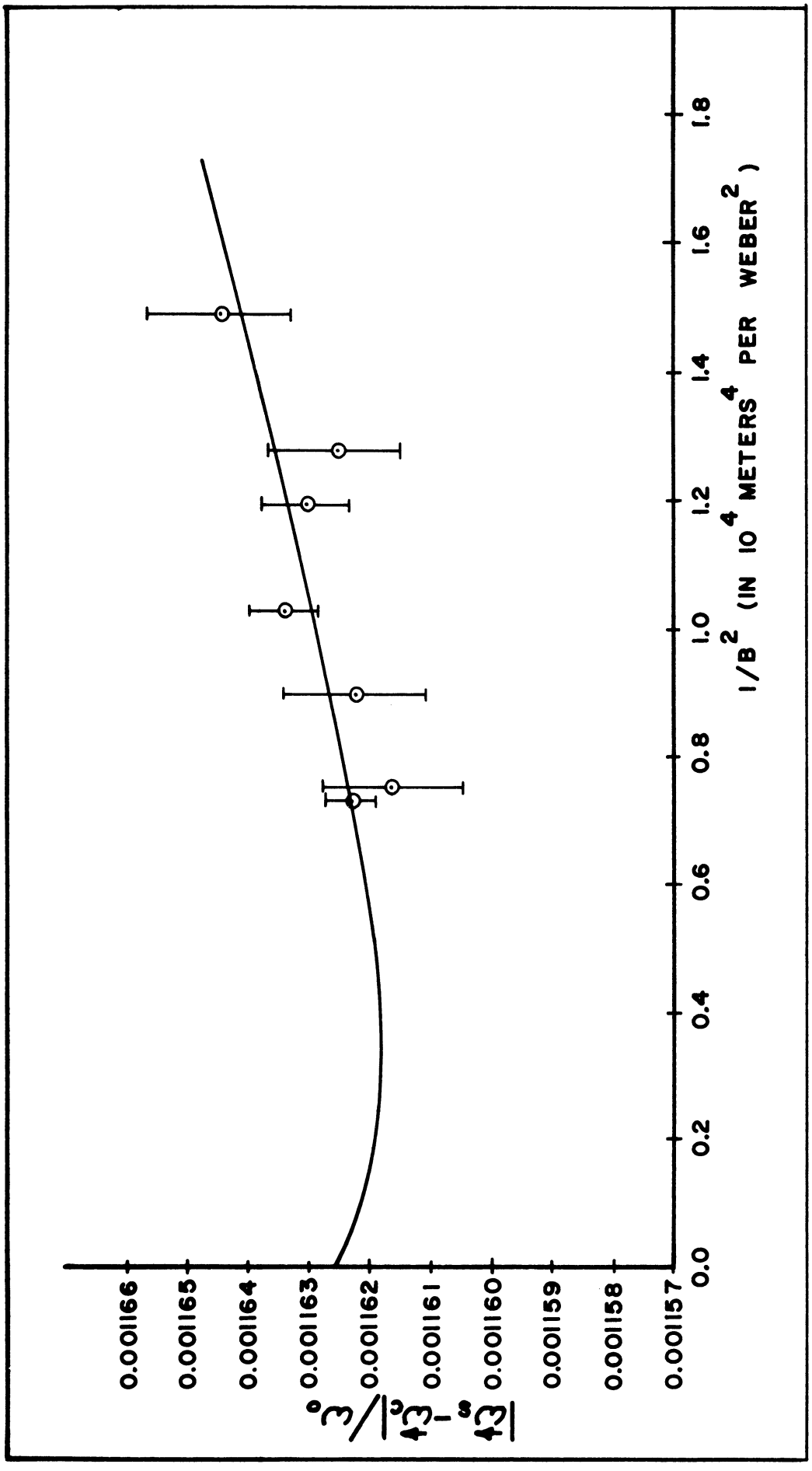

Figure 29. ω_D/ω_o Versus $1/B^2$ - Evaluation of "f"

where

a_T = theoretical value of the g-factor anomaly 0.0011596

$G = B^2 I$

$I = K^2/2a_T(K^2 + 1)$

the other factors were defined previously. Substitution of these values in (4.30) yields

$f = 8.4 \times 10^{-5}$ $\quad E = -4.8$ volts per meter.

Discussion of Errors

The quantities which may affect the final results are, 1) the mapping of the magnetic field in the trapping region, 2) the solenoid and shaping coil currents, 3) the beam energy, 4) the trapping time, 5) the stray electric field, and 6) the statistical fluctuations in the counting rates. The errors in each of these, except the last, contain a random and a systematic part. The combined effect of the random parts of all of the above errors was determined through an experimental study of the fluctuations in the phase of the double scattering asymmetry. Fifteen measurements of the phase of the double scattering asymmetry for the same experimental parameters were taken over a period of three weeks. The scatter in the results was such as to indicate a measurement of the standard deviation in the phase of 0.3 microseconds. This is the quantity labeled s_M in Equation (4.23). The standard deviation in the zero time (s_{t_o}) was determined to be 0.05 microseconds as shown in Chapter III. The standard deviation in the magnetic field was determined experimentally from the variations of the proton resonance curve observed on the oscilloscope. This included the variations in the solenoid current, the shaping coil current, and in the proton resonance device itself.

When these standard deviations are substituted in (4.23) and the square root of the sum of the squares over all runs of the same magnetic field is taken, the standard deviation for each measurement of ω_D/ω_o, shown in Table III, is obtained. These errors then propagate into the following standard deviations for the experimental results in the two cases mentioned above.

$$a = 0.0011609 \pm 0.0000011 \qquad E = -4.0 \pm 2.1 \text{ volts per meter}$$

and

$$f = (8.4 \pm 3.5) \times 10^{-5} \qquad E = -4.8 \pm 1.3 \text{ volts per meter.}$$

These errors are just the random errors present in the experimental parameters.

Systematic errors are also present in the absolute value of the magnetic field, in the trapping time, in the beam energy, and in the stray electric field. A systematic error of 0.1 percent in setting the magnetic field was found by resetting the field many times, and making an accurate measurement of the field with the proton resonance device. The voltage across the solenoid shunt was accurately reset each time with a potentiometer calibrated against a standard cell, but the magnetic field did not return to exactly the same value each time. This effect could be caused by a difference in contact potential each time the potentiometer is connected to the shunt, and by a difference in some small leakage current around the solenoid. The duration of trapping was controlled by a crystal oscillator having an absolute accuracy of 0.01 percent. The accuracy was obtained by checking the crystal against WWV. The beam energy enters into the final result only if there are stray radial electric fields in the apparatus, and then only in an insensitive

way. For the stray electric field indicated by the results, namely, about four volts per meter, a 5 percent variation in the energy would produce a change of about one part in 10^7 in the g-factor anomaly. The control of the high voltage was at least this good so that variations in the beam energy result in only about 0.01 percent variations in the measurement of the g-factor anomaly. Stray radial electric fields in the trap are an important possible source of error. They may be present due to charging of insulating films on the concentric cylinders. This field was determined, as shown earlier, by fitting the theoretical expression to the experimental points. This is an uncertain procedure, however, because it assumes that the average radial electric field was about the same for the runs at different magnetic fields. Since the stray fields represent only a few volts across the shields, a change from 100 kilovolts to about 50 kilovolts should not appreciably change the number of electrons reaching the surfaces. A day-to-day shift of the stray electric fields, due to changing of the insulating films, was ruled out because no progressive shift of the difference frequency for a given set of experimental parameters was found over a three-week period. The systematic errors may be listed as follows:

Magnetic Field	0.10%
Energy	0.01%
Time	0.01%

These errors are combined with the random errors by taking the square root of the sum of the squares. The final results with the combined errors are given in the next section.

Results and Conclusions

The evaluation of the difference frequency and magnetic field data yield the following value for the g-factor anomaly of free, high energy electrons.

$$a = 0.0011609 \pm 0.0000021 = \alpha/2\pi - (0.1 \pm 0.4)\alpha^2/\pi^2$$

where the error represents the standard deviation in the measurement. This value is in excellent agreement with the current theoretical value of

$$a = \alpha/2\pi - 0.328\alpha^2/\pi^2 = 0.0011596.$$

The data have also been evaluated to give an upper limit on the electric dipole moment of the electron. The experiment yields the following value of the f-factor of the electron

$$f = (8.4 \pm 6.7) \times 10^{-5}.$$

This places an upper limit on the electric dipole moment of

$$3 \times 10^{-15} \text{ cm (times the electronic charge).}$$

The principal sources of error are the determination of the effective magnetic field in the trapping region, the determination of the difference frequency, and the evaluation of stray fields due to charging of the concentric cylinders in the trapping region.

Suggestions for Making a More Precise Measurement

The precision of the experiment can be increased by reducing the errors mentioned above. The error in the effective value of the magnetic field is due to two different sources. The first is the absolute value of the solenoid and shaping coil fields. By using a proton resonance device to control the field, the absolute value can be held

to about one part in 10^5 which is a factor of 100 better than the value for the present experiment. The second is the determination of the time average magnetic field seen by the trapped electrons. It was found during the course of the experiment that the field inhomogeneities could be reduced to about 0.1 percent before the beam could not be trapped. By reducing this, another factor of three, the inhomogeneities would be small enough so that a measurement of the g-factor anomaly to ten times better accuracy could be made without averaging over the magnetic field. In the present experiment, no special precautions were taken to eliminate the stray electric fields. By plating the concentric cylinders and baking them in a vacuum, the stray fields can probably be reduced considerably. Also, methods are available to actually measure the electric fields. The accuracy of the determination of the difference frequency can be extended by increasing the trapping time and reducing the random and statistical errors. In this way, accuracies of one part in 10^7 or better should be possible.

APPENDIX I

TABLES OF EXPERIMENTAL RESULTS

Part A: Gold - Aluminum Scattering

For all runs: Energy 100 Kilovolts
Magnetic Field 0.8313 volts
Counts in C_2 50,000

Trapping Time	C_1	Normalized Counting Ratio	Trapping Time	C_1	Normalized Counting Ratio	Trapping Time	C_1	Normalized Counting Ratio	Trapping Time	C_1	Normalized Counting Ratio	Trapping Time	C_1	Normalized Counting Ratio
30.0	39,081	1.0035	90.0	40,934	1.0046	150.0	40,604	1.0067	210.0	40,530	0.9997	270.0	39,285	0.9782
30.5	38,365	0.9851	90.5	40,854	1.0026	150.5	40,753	1.0104	210.5	40,417	0.9970	270.5	40,422	1.0065
31.0	39,452	1.0130	91.0	40,324	0.9896	151.0	40,653	1.0079	211.0	40,515	0.9994	271.0	40,575	1.0103
31.5	38,422	0.9866	91.5	40,893	1.0036	151.5	40,007	0.9919	211.5	40,563	1.0006	271.5	39,763	0.9901
32.0	38,787	0.9960	92.0	41,034	1.0070	152.0	39,969	0.9909	212.0	40,761	1.0054	272.0	40,418	1.0064
32.5	38,547	0.9898	92.5	40,836	1.0022	152.5	40,256	0.9981	212.5	40,196	0.9915	272.5	40,262	1.0025
33.0	38,638	0.9921	93.0	40,535	0.9948	153.0	40,758	1.0105	213.0	40,742	1.0050	273.0	40,274	1.0028
33.5	38,436	0.9870	93.5	40,705	0.9990	153.5	40,241	0.9977	213.5	40,781	1.0059	273.5	40,365	1.0051
34.0	39,667	1.0186	94.0	40,519	0.9944	154.0	39,859	0.9882	214.0	40,202	0.9917	274.0	40,309	1.0037
34.5	39,607	1.0170	94.5	40,321	0.9895	154.5	40,085	0.9938	214.5	40,967	1.0105	274.5	40,381	1.0055
35.0	39,550	1.0156	95.0	40,951	1.0050	155.0	40,313	0.9995	215.0	40,715	1.0043	275.0	39,999	0.9960
35.5	39,781	1.0215	95.5	41,053	1.0075	155.5	40,510	1.0044	215.5	40,094	0.9890	275.5	39,871	0.9928
60.0	39,771	1.0007	120.0	39,953	0.9977	180.0	40,428	0.9937	240.0	40,147	0.9945	300.0	39,502	1.0002
60.5	39,692	0.9987	120.5	39,735	0.9923	180.5	40,861	1.0043	240.5	40,747	1.0094	300.5	39,489	0.9999
61.0	39,543	0.9949	121.0	39,962	0.9979	181.0	40,890	1.0050	241.0	40,864	1.0123	301.0	39,512	1.0005
61.5	39,728	0.9996	121.5	40,104	1.0015	181.5	40,796	1.0027	241.5	40,072	0.9926	301.5	39,417	0.9981
62.0	39,788	1.0011	122.0	39,867	0.9956	182.0	41,045	1.0088	242.0	40,689	1.0079	302.0	39,370	0.9969
62.5	39,662	0.9979	122.5	40,182	1.0034	182.5	40,883	1.0048	242.5	40,507	1.0034	302.5	39,531	1.0010
63.0	39,745	1.0000	123.0	40,039	0.9998	183.0	40,720	1.0008	243.0	40,026	0.9915	303.0	39,560	1.0017
63.5	39,781	1.0009	123.5	40,201	1.0039	183.5	40,251	0.9893	243.5	39,896	0.9883	303.5	39,354	0.9965
64.0	39,673	0.9982	124.0	40,075	1.0007	184.0	40,783	1.0024	244.0	40,504	1.0033	304.0	39,546	1.0014
64.5	39,904	1.0040	124.5	39,782	0.9934	184.5	40,337	0.9914	244.5	40,411	1.0010	304.5	39,537	1.0011
65.0	39,784	1.0010	125.0	40,278	1.0058	185.0	40,651	0.9991	245.0	40,462	1.0023	305.0	39,520	1.0007
65.5	39,852	1.0027	125.5	40,362	1.0079	185.5	40,590	0.9976	245.5	40,104	0.9934	305.5	39,543	1.0013

Part B: Gold - Gold Scattering

Energy - 100 Kilovolts Magnetic Field - 0.8313 Volts

Trapping Time	C_1	Normalized Counting Ratio	Trapping Time	C_1	Normalized Counting Ratio	Trapping Time	C_1	Normalized Counting Ratio
	Run I C_2 = 20,000			Run III C_2 = 20,000			Run V C_2 = 20,000	
30.0	17,232	1.0311	90.0	17,543	1.0071	150.0	17,678	1.0091
30.5	16,828	1.0069	90.5	17,289	0.9925	150.5	17,949	1.0245
31.0	16,658	0.9968	91.0	16,746	0.9614	151.0	16,935	0.9667
31.5	17,113	1.0240	91.5	17,431	1.0007	151.5	17,465	0.9969
32.0	16,933	1.0132	92.0	17,629	1.0121	152.0	17,427	0.9947
32.5	16,780	1.0041	92.5	17,719	1.0172	152.5	17,904	1.0220
33.0	16,143	0.9660	93.0	17,382	0.9978	153.0	17,673	1.0088
33.5	16,113	0.9642	93.5	17,138	0.9839	153.5	17,000	0.9704
34.0	16,499	0.9873	94.0	17,039	0.9782	154.0	17,012	0.9711
34.5	17,107	1.0236	94.5	17,587	1.0096	154.5	17,693	1.0099
35.0	16,688	0.9986	95.0	18,087	1.0383	155.0	17,797	1.0159
35.5	16,447	0.9841	95.5	17,442	1.0013	155.5	17,695	1.0100
	Run II			Run IV			Run VI	
60.0	17,095	0.9919	120.0	17,278	0.9875	180.0	17,411	0.9863
60.5	17,340	1.0061	120.5	17,512	1.0009	180.5	17,640	0.9992
61.0	17,634	1.0232	121.0	17,686	1.0108	181.0	18,077	1.0240
61.5	17,250	1.0009	121.5	17,521	1.0014	181.5	18,008	1.0201
62.0	16,398	0.9514	122.0	17,443	0.9969	182.0	17,676	1.0013
62.5	17,394	1.0092	122.5	17,163	0.9809	182.5	17,289	0.9793
63.0	17,135	0.9942	123.0	17,643	1.0083	183.0	17,608	0.9974
63.5	17,483	1.0144	123.5	17,767	1.0154	183.5	18,016	1.0205
64.0	17,513	1.0161	124.0	17,954	1.0261	184.0	18,081	1.0242
64.5	17,096	0.9919	124.5	17,446	0.9971	184.5	17,551	0.9942
65.0	16,996	0.9861	125.0	17,269	0.9870	185.0	17,044	0.9655
65.5	17,486	1.0146	125.5	17,281	0.9877	185.5	17,443	0.9881

Part B (Continued)

Energy - 100 Kilovolts Magnetic Field - 0.8313 Volts

Trapping Time	C_1	Normalized Counting Ratio	Trapping Time	C_1	Normalized Counting Ratio	Trapping Time	C_1	Normalized Counting Ratio	Trapping Time	C_1	Normalized Counting Ratio
Run VII C_2 = 20,000			Run IX C_2 = 20,000			Run XI C_2 = 20,000			Run XIII C_2 = 30,000		
210.0	17,782	1.0188	270.0	18,538	1.0193	300.0	17,324	0.9979	300.0	25,888	1.0090
210.5	17,522	1.0039	270.5	18,277	1.0049	300.5	16,973	0.9777	300.5	25,206	0.9824
211.0	17,213	0.9862	271.0	17,850	0.9814	301.0	17,358	0.9999	301.0	25,360	0.9884
211.5	16,958	0.9716	271.5	17,719	0.9742	301.5	17,372	1.0007	301.5	25,863	1.0080
212.0	17,135	0.9817	272.0	17,681	0.9722	302.0	17,889	1.0305	302.0	26,350	1.0270
212.5	17,514	1.0035	272.5	18,146	0.9977	302.5	17,542	1.0105	302.5	25,938	1.0110
213.0	18,072	1.0354	273.0	18,822	1.0349	303.0	17,281	0.9955	303.0	25,123	0.9792
213.5	17,496	1.0024	273.5	18,404	1.0119	303.5	16,988	0.9786	303.5	25,114	0.9788
214.0	16,945	0.9709	274.0	18,261	1.0040	304.0	17,388	1.0016	304.0	25,510	0.9943
214.5	17,447	0.9996	274.5	17,780	0.9776	304.5	17,936	1.0332	304.5	26,179	1.0204
215.0	17,711	1.0147	275.0	18,102	0.9953	305.0	17,471	1.0064	305.0	25,904	1.0096
215.5	17,650	1.0112	275.5	18,669	1.0265	305.5	16,794	0.9674	305.5	25,446	0.9918
Run VIII			Run X			Run XII					
240.0	17,090	0.9627	300.0	17,563	0.9799	300.0	17,381	0.9994			
240.5	17,472	0.9842	300.5	17,462	0.9743	300.5	17,074	0.9817			
241.0	18,282	1.0299	301.0	18,255	1.0185	301.0	17,369	0.9987			
241.5	18,678	1.0522	301.5	18,030	1.0059	301.5	17,481	1.0051			
242.0	17,684	0.9962	302.0	18,574	1.0313	302.0	17,992	1.0345			
242.5	17,390	0.9796	302.5	17,941	1.0010	302.5	17,516	1.0071			
243.0	17,293	0.9742	303.0	18,066	1.0080	303.0	17,275	0.9933			
243.5	18,190	1.0247	303.5	17,652	0.9849	303.5	17,022	0.9737			
244.0	18,153	1.0226	304.0	18,251	1.0183	304.0	17,448	1.0032			
244.5	17,883	1.0074	304.5	18,622	1.0390	304.5	17,906	1.0295			
245.0	17,530	0.9875	305.0	17,725	0.9886	305.0	17,375	0.9990			
245.5	17,375	0.9788	305.5	16,939	0.9451	305.5	16,864	0.9696			

Part B (Continued)

Trapping Time	C_1	Normalized Counting Ratio
Run XIV C_2 = 40,000 Energy - 98 Kilovolts Magnetic Field - 0.8212 Volts		
300.0	35,355	1.0102
300.5	35,842	1.0241
301.0	34,838	0.9954
301.5	34,101	0.9743
302.0	34,134	0.9753
302.5	35,270	1.0077
303.0	35,532	1.0152
303.5	35,016	1.0005
304.0	34,639	0.9897
304.5	34,384	0.9824
305.0	34,991	0.9998
305.5	35,885	1.0253
Run XV Energy - 81 Kilovolts Magnetic Field - 0.7500 Volts		
300.0	37,299	1.0190
300.5	35,873	0.9800
301.0	35,662	0.9743
301.5	35,750	0.9767
302.0	36,690	1.0024
302.5	37,005	1.0110
303.0	37,209	1.0165
303.5	36,528	0.9979
304.0	36,151	0.9876
304.5	36,709	1.0029
305.0	36,978	1.0102
305.5	37,388	1.0214

Trapping Time	C_1	Normalized Counting Ratio
Run XVI C_2 = 40,000 Energy - 70 Kilovolts Magnetic Field - 0.7000 Volts		
200.0	34,300	1.0062
200.5	34,193	1.0031
201.0	33,975	0.9967
201.5	33,606	0.9859
202.0	34,123	1.0010
202.5	34,269	1.0053
203.0	34,747	1.0193
203.5	34,504	1.0122
204.0	33,959	0.9962
204.5	33,574	0.9849
205.0	33,632	0.9866
205.5	34,179	1.0027
Run XVII		
250.0	38,893	1.0017
250.5	38,361	0.9880
251.0	38,356	0.9879
251.5	38,804	0.9994
252.0	39,463	1.0164
252.5	39,397	1.0147
253.0	38,838	1.0003
253.5	38,475	0.9909
254.0	38,254	0.9852
254.5	38,714	0.9971
255.0	38,965	1.0036
255.5	39,403	1.0148

Trapping Time	C_1	Normalized Counting Ratio
Run XVIII C_2 = 40,000 Energy - 70 Kilovolts Magnetic Field - 0.7000 Volts		
265.0	39,238	1.0124
265.5	39,259	1.0130
266.0	38,696	0.9984
266.5	38,060	0.9821
267.0	38,371	0.9901
267.5	38,718	0.9990
268.0	39,288	1.0137
268.5	39,033	1.0072
269.0	39,079	1.0083
269.5	38,395	0.9907
270.0	38,321	0.9888
270.5	38,609	0.9962
Run XIX		
285.0	34,138	0.9937
285.5	33,874	0.9860
286.0	34,762	1.0119
286.5	34,332	0.9994
287.0	33,902	0.9868
287.5	33,622	0.9787
288.0	34,340	0.9996
288.5	34,245	0.9968
289.0	35,335	1.0286
289.5	34,808	1.0132
290.0	34,689	1.0097
290.5	34,190	0.9952

Trapping Time	C_1	Normalized Counting Ratio
Run XX C_2 = 40,000 Energy - 70 Kilovolts Magnetic Field - 0.7000 Volts		
300.0	38,405	0.9892
300.5	37,931	0.9770
301.0	38,422	0.9896
301.5	38,793	0.9992
302.0	39,285	1.0118
302.5	39,063	1.0061
303.0	38,964	1.0036
303.5	38,581	0.9937
304.0	38,548	0.9929
304.5	39,226	1.0103
305.0	39,338	1.0132
305.5	39,349	1.0135

Part B (Continued)

Trapping Time	C_1	Normalized Counting Ratio	Trapping Time	C_1	Normalized Counting Ratio	Trapping Time	C_1	Normalized Counting Ratio
Run XXI C_2 = 40,000 Energy - 60 Kilovolts Magnetic Field - 0.6500 Volts			Run XXIII C_2 = 40,000 Energy - 60 Kilovolts Magnetic Field - 0.6500 Volts			Run XXV C_2 = 40,000 Energy - 50 Kilovolts Magnetic Field - 0.5819 Volts		
250.0	37,962	0.9943	300.0	38,585	0.9865	300.0	36,543	1.0141
250.5	38,118	0.9984	300.5	38,818	0.9925	300.5	36,256	1.0061
251.0	37,699	0.9875	301.0	39,683	1.0146	301.0	35,736	0.9917
251.5	37,805	0.9902	301.5	39,527	1.0106	301.5	35,406	0.9825
252.0	38,492	1.0082	302.0	39,553	1.0113	302.0	36,367	1.0092
252.5	38,667	1.0128	302.5	39,244	1.0034	302.5	36,041	1.0001
253.0	38,112	0.9983	303.0	38,926	0.9953	303.0	36,038	1.0000
253.5	37,745	0.9887	303.5	38,713	0.9898	303.5	36,672	1.0176
254.0	37,891	0.9925	304.0	38,701	0.9895	304.0	36,056	1.0005
254.5	38,592	1.0108	304.5	39,044	0.9983	304.5	35,821	0.9940
255.0	38,684	1.0133	305.0	39,297	1.0048	305.0	35,512	0.9855
255.5	38,368	1.0050	305.5	39,242	1.0033	305.5	35,986	0.9986
Run XXII			Run XXIV Energy - 58 Kilovolts Magnetic Field - 0.6286 Volts					
300.0	34,708	0.9915	300.0	40,563	0.9946			
300.5	34,786	0.9937	300.5	40,118	0.9836			
301.0	34,713	0.9917	301.0	41,283	1.0122			
301.5	35,542	1.0153	301.5	41,074	1.0071			
302.0	34,977	0.9992	302.0	41,102	1.0078			
302.5	35,227	1.0063	302.5	40,802	1.0004			
303.0	34,830	0.9950	303.0	40,353	0.9894			
303.5	34,286	0.9795	303.5	40,201	0.9857			
304.0	35,159	1.0044	304.0	39,979	0.9802			
304.5	35,197	1.0055	304.5	41,379	1.0147			
305.0	35,181	1.0050	305.0	40,340	0.9801			
305.5	35,451	1.0127	305.5	40,425	0.9912			

Part C: Continuous Run from 30 to 130 Microseconds

Energy - 95 Kilovolts Magnetic Field - 0.8000 Volts

Trapping Time	C_1	C_2	Trapping Time	C_1	C_2	Trapping Time	C_1	C_2	Trapping Time	C_1	C_2	Trapping Time	C_1	C_2
30.0	28,100	50,000	50.0	6,154	10,000	70.0	6,002	10,000	90.0	5,828	10,000	110.0	5,842	10,000
30.5	28,559	50,000	50.5	6,083	10,000	70.5	6,254	10,000	90.5	5,873	10,000	110.5	5,734	10,000
31.0	28,400	50,000	51.0	5,823	10,000	71.0	6,342	10,000	91.0	5,579	10,000	111.0	5,572	10,000
31.5	27,753	50,000	51.5	5,779	10,000	71.5	6,131	10,000	91.5	5,644	10,000	111.5	5,810	10,000
32.0	27,822	50,000	52.0	6,052	10,000	72.0	6,023	10,000	92.0	5,590	10,000	112.0	5,912	10,000
32.5	28,210	50,000	52.5	6,199	10,000	72.5	5,936	10,000	92.5	5,570	10,000	112.5	6,028	10,000
33.0	29,130	50,000	53.0	6,081	10,000	73.0	5.959	10,000	93.0	5,721	10,000	113.0	5,822	10,000
33.5	28,914	50,000	53.5	5,931	10,000	73.5	6,059	10,000	93.5	5,721	10,000	113.5	5,649	10,000
34.0	28,217	50,000	54.0	6,178	10,000	74.0	6,102	10,000	94.0	5,492	10,000	114.0	5,750	10,000
34.5	5,696	10,000	54.5	6,140	10,000	74.5	6,169	10,000	94.5	5,381	10,000	114.5	6,148	10,000
35.0	5,626	10,000	55.0	6,084	10,000	75.0	6,091	10,000	95.0	5,898	10,000	115.0	5,941	10,000
35.5	5,800	10,000	55.5	6,099	10,000	75.5	5,735	10,000	95.5	6,039	10,000	115.5	6,003	10,000
36.0	5,887	10,000	56.0	6,163	10,000	76.0	5,983	10,000	96.0	6,097	10,000	116.0	5,959	10,000
36.5	5,959	10,000	56.5	5,909	10,000	76.5	6,093	10,000	96.5	5,926	10,000	116.5	5,824	10,000
37.0	5,771	10,000	57.0	6,141	10,000	77.0	5,981	10,000	97.0	5,666	10,000	117.0	5,820	10,000
37.5	5,683	10,000	57.5	6,007	10,000	77.5	6,002	10,000	97.5	5,876	10,000	117.5	6,117	10,000
38.0	5,781	10,000	58.0	6,383	10,000	78.0	5,878	10,000	98.0	5,939	10,000	118.0	5,952	10,000
38.5	6,033	10,000	58.5	6,142	10,000	78.5	5,845	10,000	98.5	5,771	10,000	118.5	5,887	10,000
39.0	6,014	10,000	59.0	5,880	10,000	79.0	5,997	10,000	99.0	5,920	10,000	119.0	5,732	10,000
39.5	5,885	10,000	59.5	6,052	10,000	79.5	5,815	10,000	99.5	5,674	10,000	119.5	5,996	10,000
40.0	5,825	10,000	60.0	6,126	10,000	80.0	5,938	10,000	100.0	5,480	10,000	120.0	6,055	10,000
40.5	5,829	10,000	60.5	6,274	10,000	80.5	5,703	10,000	100.5	5,652	10,000	120.5	6,060	10,000
41.0	5,900	10,000	61.0	6,282	10,000	81.0	5,644	10,000	101.0	5,852	10,000	121.0	5,947	10,000
41.5	5,863	10,000	61.5	6,219	10,000	81.5	5,890	10,000	101.5	5,837	10,000	121.5	5,929	10,000
42.0	5,976	10,000	62.0	6,187	10,000	82.0	5,799	10,000	102.0	5,701	10,000	122.0	6,032	10,000
42.5	5,835	10,000	62.5	6,181	10,000	82.5	5,796	10,000	102.5	5,511	10,000	122.5	6,078	10,000
43.0	5,810	10,000	63.0	6,148	10,000	83.0	5,760	10,000	103.0	5,672	10,000	123.0	6,311	10,000
43.5	5,863	10,000	63.5	6,217	10,000	83.5	5,503	10,000	103.5	5,672	10,000	123.5	6,221	10,000
44.0	6,010	10,000	64.0	6,375	10,000	84.0	5,503	10,000	104.0	5,759	10,000	124.0	5,958	10,000
44.5	6,238	10,000	64.5	6,010	10,000	84.5	5,563	10,000	104.5	5,545	10,000	124.5	5,962	10,000
45.0	6,060	10,000	65.0	5,961	10,000	85.0	5,731	10,000	105.0	5,660	10,000	125.0	6,000	10,000
45.5	5,759	10,000	65.5	6,221	10,000	85.5	5,552	10,000	105.5	5,345	10,000	125.5	6,300	10,000
46.0	5,806	10,000	66.0	6,328	10,000	86.0	5,373	10,000	106.0	5,580	10,000	126.0	31,161	50,000
46.5	5,966	10,000	66.5	6,184	10,000	86.5	5,511	10,000	106.5	5,728	10,000	126.5	30,492	50,000
47.0	6,232	10,000	67.0	6,084	10,000	87.0	5,543	10,000	107.0	5,799	10,000	127.0	30,424	50,000
47.5	5,983	10,000	67.5	5,995	10,000	87.5	5,528	10,000	107.5	5,623	10,000	127.5	29,922	50,000
48.0	5,852	10,000	68.0	6,029	10,000	88.0	5,785	10,000	108.0	5,593	10,000	128.0	30,478	50,000
48.5	5,916	10,000	68.5	6,212	10,000	88.5	5,496	10,000	108.5	5,677	10,000	128.5	31,023	50,000
49.0	5,942	10,000	69.0	6,131	10,000	89.0	5,380	10,000	109.0	5,773	10,000	129.0	31,355	50,000
49.5	6,018	10,000	69.5	6,117	10,000	89.5	5,345	10,000	109.5	5,915	10,000	129.5	30,734	50,000
												130.0	30,114	50,000

APPENDIX II

TABLES OF CALCULATED VALUES

Part A: Calculated Values of Magnetic Field Due to the Solenoid and Field Shaping Coil

Solenoid Dimensions: 5.792 Meters Long
0.338 Meters Diameter
1492 Turns per Meter

Field Shaping Coil Dimensions: 0.154 Meters Long
0.464 Meters Diameter
593 Turns Total

Fields Calculated for a Beam Radius of 0.095 Meters

Z From Center	Solenoid		Shaping Coil	
	Axial Field 10^{-4} W/M^2	Radial Field 10^{-6} W/M^2	Axial Field 10^{-4} W/M^2	Radial Field 10^{-6} W/M^2
0.000	117.3900	0.00000	0.32000	0.00000
0.025	---	---	---	1.70324
0.050	117.3893	0.03061	0.28387	3.40638
0.075	---	---	---	4.54194
0.100	117.3886	0.06124	0.22967	5.26450
0.125	---	---	---	5.41927
0.150	117.3880	0.09185	0.16516	5.05800
0.200	117.3874	0.12397	0.12129	3.87091
0.250	117.3855	0.15687	0.08774	2.73545
0.300	117.3836	0.18979	0.06193	1.96127
0.350	117.3808	---	0.04387	1.39359
0.400	117.3780	0.26041	0.03200	1.03221
0.450	117.3746	---	0.02479	0.72256
0.500	117.3711	0.33784	0.01909	0.48510
0.550	117.3665	---	0.01549	0.34069
0.600	117.3617	0.45584	0.01238	0.20640
0.650	117.3570	---	0.00878	0.15488
0.700	117.3523	0.52324	0.00722	0.10325
0.800	117.3385	0.63784	0.00516	0.05163
0.900	117.3228	0.77315	---	---
1.000	117.3027	0.93544	---	---
1.100	117.2789	1.22691	---	---
1.200	117.2507	1.37855	---	---
1.300	117.2174	1.68771	---	---
1.400	117.1741	2.08455	---	---

Part B: Calculated Values of Effective Potential Well

Z	Electron Volts	Z	Electron Volts
1.45	141.24	0.70	3.63
1.40	124.16	0.65	1.49
1.35	108.65	0.60	0.41
1.30	94.63	0.55	0.00
1.25	81.84	0.50	1.90
1.20	70.13	0.45	5.78
1.15	59.57	0.40	12.13
1.10	50.08	0.35	22.19
1.05	41.50	0.30	37.04
1.00	33.83	0.25	59.32
0.95	26.98	0.20	90.09
0.90	20.87	0.15	131.18
0.85	15.43	0.10	174.74
0.80	10.73	0.05	204.52
0.75	6.77	0.00	217.93

BIBLIOGRAPHY

1. Lamb, W. E., Jr. and Retherford, R. C. Phys. Rev., 72, (1947), 241; 79, (1950), 549; 81, (1951), 222. Lamb, W. E. Jr. Phys. Rev., 85, (1952), 259. Lamb, W. E., Jr. and Retherford, R. C. Phys. Rev., 86, (1952), 1014. Triebwasser, S., Dayhoff, E. S., and Lamb, W. E., Jr. Phys. Rev., 89, (1953), 106.

2. Dirac, P. A. M. Proc. Roy. Soc., (London), A 117, (1928), 610; A 118, (1928), 351.

3. Bethe, H. A. Phys. Rev., 72, (1947), 339

4. Breit, G. Phys. Rev., 72, (1947), 984.

5. Nafe, J. E., Nelson, E. B., and Rabi, I. I. Phys. Rev., 71, (1947), 914.

6. Nagle, D. E., Julian, R. S., and Zacharas, J. R. Phys. Rev., 72, (1947), 971.

7. Schwinger, J. Phys. Rev., 73, (1948), 416.

8. Schwinger, J. Phys. Rev., 74, (1948), 1439; 75, (1949), 651; 76, (1949), 790.

9. Cohen, E. R. and DuMond, J. W. M. Phys. Rev. Letters, 1, (1958), 291.

10. Karplus, R. and Kroll, N. M. Phys. Rev., 77, (1950), 536.

11. Sommerfield, C. M. Phys. Rev., 107, (1957), 328.

12. Petermenn, A. Nuclear Physics, 5, (1958), 677.

13. Kusch, P. and Foley, H. M. Phys. Rev., 74, (1949), 1481.

14. Taub, H. and Kusch, P. Phys. Rev., 75, (1949), 1481.

15. Kusch, P. and Taub, H. Phys. Rev., 75, (1949), 1477.

16. Koenig, S. H., Prodell, A. G., and Kusch, P. Phys. Rev., 88, (1952), 191.

17. Beringer, R. and Heald, M. A. Phys. Rev., 95, (1954), 1474.

18. Geiger, J. S., Hughes, V. W., and Radford, H. E. Phys. Rev., 105, (1957), 183.

19. Gardner, J. H. and Purcell, E. M. Phys. Rev., 76, (1949), 1262; Gardner, J. H. Phys. Rev., 83, (1951), 996.

20. Franken, P. and Liebes, S., Jr. Phys. Rev., 104, (1956), 1197; Private Communication.

21. Hardy, W. and Purcell, E. M. Private Communication, 1958.

22. Bloch, F. Physica, 19, (1953), 821.

23. Mott, N. F. Proc. Roy. Soc., (London), A 124, (1929), 425.

24. Nelson, D. F. Ph.D. Thesis, University of Michigan, Ann Arbor, Michigan, 1958. (Unpublished).

25. Tolhoek, H. A. and DeGroot, S. R. Physica, 17, (1951), 17.

26. Crane, H. R., Pidd, R. W., and Louisell, W. H. Phys. Rev., 91, (1953), 475.

27. Louisell, W. H., Pidd, R. W., and Crane, H. R. Phys. Rev., 94, (1954), 7; Louisell, W. H. Ph.D. Thesis, University of Michigan, Ann Arbor, Michigan, 1953. (Unpublished).

28. Mendlowitz, H. and Case, K. M. Phys. Rev., 97, (1955), 33; 100, (1955), 1551. Mendlowitz, H. Ph.D. Thesis, University of Michigan, Ann Arbor, Michigan, 1954. (Unpublished).

29. Smythe, W. R. Static and Dynamic Electricity. New York: McGraw-Hill Book Co., 1950, Chapter VII, 270.

30. Ford, G. W. Private Communication, 1959.

31. Salpeter, E. E. Phys. Rev., 112, (1958), 1642.